DYNAMICS FOR CHAOS AND FRACTALS

A THESIS SUBMITTED TO
THE GRADUATE SCHOOL OF NATURAL AND APPLIED SCIENCES
OF
MIDDLE EAST TECHNICAL UNIVERSITY

BY

EJAILY ALEJAILY

IN PARTIAL FULFILLMENT OF THE REQUIREMENTS
FOR
THE DEGREE OF DOCTOR OF PHILOSOPHY
IN
MATHEMATICS

AUGUST 2019

Approval of the thesis:

DYNAMICS FOR CHAOS AND FRACTALS

submitted by **EJAILY ALEJAILY** in partial fulfillment of the requirements for the degree of **Doctor of Philosophy in Mathematics Department, Middle East Technical University** by,

Prof. Dr. Halil Kalıpçılar
Dean, Graduate School of **Natural and Applied Sciences**　———————

Prof. Dr. Yıldıray Ozan
Head of Department, **Mathematics**　———————

Prof. Dr. Marat Akhmet
Supervisor, **Mathematics Department, METU**　———————

Assoc. Prof. Dr. Mehmet Onur Fen
Co-supervisor, **Mathematics Department, TED University**　———————

Examining Committee Members:

Prof. Dr. Hurşit Önsiper
Mathematics Department, METU　———————

Prof. Dr. Marat Akhmet
Mathematics Department, METU　———————

Prof. Dr. Hüseyin Bereketoğlu
Mathematics Department, Ankara University　———————

Assoc. Prof. Dr. Fatma Fen
Mathematics Department, Gazi University　———————

Assoc. Prof. Dr. Duygu Aruğaslan
Mathematics Department, Süleyman Demirel University　———————

Date:

I hereby declare that all information in this document has been obtained and presented in accordance with academic rules and ethical conduct. I also declare that, as required by these rules and conduct, I have fully cited and referenced all material and results that are not original to this work.

Name, Surname: Ejaily Alejaily

Signature   :

ABSTRACT

DYNAMICS FOR CHAOS AND FRACTALS

Alejaily, Ejaily

Ph.D., Department of Mathematics

Supervisor: Prof. Dr. Marat Akhmet

Co-Supervisor: Assoc. Prof. Dr. Mehmet Onur Fen

August 2019, 98 pages

In this thesis, we study how to construct and analyze dynamics for chaos and fractals. After the introductory chapter, we discuss in the second chapter the chaotic behavior of hydrosphere parameters and their influence on global weather and climate. For this purpose, we investigate the nature and source of unpredictability in the dynamics of sea surface temperature. The impact of sea surface temperature variability on the global climate is clear during some global climate patterns like the El Niño-Southern Oscillation. The interactions between these types of global climate patterns may transmit chaos. We discuss the unpredictability as a global phenomenon through extension of chaos *horizontally* and *vertically* by using theoretical as well as numerical analyses. In the third chapter, we introduce a technique concerning the construction of dynamics for fractals. Deterministic fractals like Julia sets are crucial for understanding the fractal phenomenon. These structures are deterministically arising from simple dynamics of iteration of analytic functions. On the basis of the dynamics, we develop a scheme to map fractals through iterations. This allows to involve fractals as states of dynamical systems as well as to introduce dynamics in fractals through differential and discrete equations. Creation of effective frameworks

for applications of fractals and assisting to explore the relationship between fractals and chaos by the involvement of dynamics in fractals are important aspects in this direction.

ÖZ

KAOS VE FRAKTALLAR İÇİN DİNAMİKLER

Alejaily, Ejaily

Doktora, Matematik Bölümü

Tez Yöneticisi: Prof. Dr. Marat Akhmet

Ortak Tez Yöneticisi: Doç. Dr. Mehmet Onur Fen

Ağustos 2019 , 98 sayfa

Bu tezde kaos ve fraktallar için dinamiklerin nasıl oluşturulacağını ve analiz edileceğini çalışmaktayız. Giriş bölümünden sonra, ikinci bölümde hidrosfer parametrelerinin kaotik davranışını ve küresel hava ve iklim üzerine etkisini tartışmaktayız. Bu amaçla, deniz yüzeyi sıcaklığı dinamiğinde öngörülemezliğin doğasını ve kaynağını araştırmaktayız. Deniz yüzeyi sıcaklığı değişkenliğinin küresel iklim üzerindeki etkisi El Niño-Güney Salınımı gibi bazı küresel iklim örüntüleri süresince belirgindir. Bu türdeki küresel iklim örüntüleri arasındaki etkileşimler kaosu iletebilir. Öngörülemezliği küresel bir olgu olarak kaosun yatay ve dikey genişlemesi aracılığıyla hem teorik hem de sayısal analiz kullanarak tartışmaktayız. Üçüncü bölümde, fraktallar için dinamiklerin oluşturulmasına ilişkin bir teknik tanıtmaktayız. Julia kümeleri gibi rastgele olmayan fraktallar, fraktal olgusunun anlaşılması için çok önemlidir. Bu yapılar analitik fonksiyonların iterasyonunun basit dinamiğinden deterministik bir şekilde kaynaklanmaktadır. Dinamiklere dayanılarak iterasyonlar yoluyla fraktalların gönderimi için bir şema geliştirmekteyiz. Bu, fraktalların dinamik sistemlerin halleri olarak kapsanmasının yanı sıra diferansiyel ve ayrık denklemler aracılığıyla fraktallarda dinamiğin tanıtılmasına izin vermektedir. Fraktallarda dinamiklerin içerilmesinin frak-

talların uygulamaları için etkili bir çerçeve meydana getirmesi ve fraktallarla kaos arasındaki ilişkinin araştırılması için faydalı olması bu yöndeki önemli taraflardır.

Anahtar Kelimeler: Kaos, Okyanus-atmosfer etkileşimi, El Niño-güney salınımı, Deniz yüzeyi sıcaklığı, Vallis modeli, Lorenz sistemi, Adveksiyon denklemi, Küresel hava öngörülemezliği, Fraktallar, Julia kümesi, Mandelbrot kümesi, Fatou-Julia iterasyonu, Sierpinski fraktalları, Fraktal gönderimleri, Ayrık ve sürekli fraktal dinamiği, Duffing denklemi, Van der Pol denklemi

To my family

ACKNOWLEDGMENTS

First, I would like to thank my supervisor Prof. Dr. Marat Akhmet for his precious guidance, continuous encouragement and persuasive support throughout the research. I also would like to express my gratitude to my co-supervisor Associate Professor Mehmet Onur Fen, for his valuable guidance and support throughout the preparation of this thesis.

I offer my sincere gratitude to the members of the examining committee and also to all members of the Mathematics Department of Middle East Technical University for their help during my PhD studies.

Finally, I would like to thank all the people who contributed to the work described in this thesis.

TABLE OF CONTENTS

LIST OF TABLES

TABLES

LIST OF FIGURES

FIGURES

LIST OF ALGORITHMS

ALGORITHMS

LIST OF ABBREVIATIONS

AMO   Atlantic Multidecadal Oscillation

AO   Arctic Oscillation

ENSO   El Niño and Southern Oscillation

IFS   Iterated Function Systems

IOD   Indian Ocean Dipole

FJI   Fatou-Julia Iteration

FMI   Fractals Mapping Iteration

FMT   Fractal Mapping Theorem

MJO   Madden-Julian Oscillation

NAM   Northern Annular Mode

NAO   North Atlantic Oscillation

PDO   Pacific Decadal Oscillation

PNA   Pacific/North American pattern

QBO   Quasi-Biennial Oscillation

SST   Sea Surface Temperature

TAV   Tropical Atlantic Variability

WP   Western Pacific pattern

CHAPTER 1

INTRODUCTION

1.1   Chaos and Fractals

Chaos and fractals are interesting fields of scientific research in mathematics, physics, engineering and many other branches of sciences. They provide us with powerful mathematical tools to analyze and understand the irregularity and complexity of many natural and artificial phenomena. Fractal geometry is older than chaos theory, however, the mathematical terms "*chaos*" and "*fractal*" are Irish twins. Tien-Yien Li and James Yorke [1] use the word "*chaos*" in 1975 to describe an irregular behavior of certain type of dynamical systems, whereas the word "*fractal*" was coined by Benoit Mandelbrot [2] in the same year, refers to certain geometrical structures.

1.1.1   Chaos Phenomenon

Chaos, in general, can be defined as aperiodic long-term behavior in a deterministic system that exhibits sensitive dependence on initial conditions [3, 4]. The first recognition of chaos phenomenon was indicated in the work of Henri Poincarè in the late 19th century, when he studied the problem of the stability of the solar system. The property of unpredictability appears in planets' motions through models used to predict their future position. The roots of the problem date back to the last quarter of the eighteenth century when Laplace tried to prove the stability of the planetary system. Using Newton's laws, Laplace developed a perturbation theory to describe planet's orbit around the Sun. He concluded that the solar system is stable and the paths of planets can be reliably predicted far into the future as well as described far into the past [5]. However, Laplace made some simplifying assumptions relating to

the mutual gravitational attraction between the planets, and so his result cannot be considered as the final word on the subject [6]. Poincaré studied the same problem, and in 1890 he showed that a gravitational system admits the possibility of unpredictable solution even for a system involving only three bodies [7, 8]. Indeed, during the latter half of the 20th century and because of computer revolution, unpredictability (chaotic behavior) in the motion of planets became a more realistic assumption. Consequentially, prediction of the future position of the planets may introduce great difficulties. In the late 1980s, Sussman, Wisdom and Laskar [9, 10, 11] showed numerically that the solar system is chaotic (sensitive to initial conditions). An error of 150 meters in the position of the Earth today may led to an error of 150 million kilometers after 100 million years [12].

The property of *sensitive dependence on initial conditions* was firstly discovered in the 1950s by Edward Lorenz during his investigation into some weather forecasting models [13]. The discovery contributed significantly to give an interpretation why is it very difficult to forecast the weather for more than 10 days in advance. Weather forecasting models are extremely sensitive to initial conditions. This sensitivity means that slight deviation in the initial state may cause an unpredictably large change in the final state. This phenomenon is popularly called "butterfly effect".

The sensitivity property is considered as the main ingredient of chaos. There are different types and definitions of chaos. Devaney [14] and Li-Yorke [1] chaos are the most frequently used types, which are characterized by transitivity, sensitivity, frequent separation and proximality. Another common type occurs through period-doubling cascade which is a sort of route to chaos through local bifurcations [15, 16, 17]. In the papers [18, 19], Poincaré chaos was introduced through the unpredictable point concepts. Further, it was developed to unpredictable functions and sequences.

1.1.2 Fractals Geometry

Fractal geometry is a mathematical tool used to describe many natural structures that adopt various degrees of *self-similarity*, as well as to design some artificial structures. A set that displays self-similarity and repeats the same patterns at every scale is usually called fractal. Mandelbrot defined a fractal as a set for which the Hausdorff

dimension strictly exceeds the topological dimension [20]. Dealing with fractals goes back to the 17th Century when Gottfried Leibniz introduced notions of recursive self-similarity [21]. Since then, history has not recorded any thing about self-similarity until the late 19th century when Karl Weierstrass introduced in 1872 a function that being everywhere continuous but nowhere differentiable. The graph of the Weierstrass function became an example of a self-similar fractal. The Cantor set, constructed by Georg Cantor in 1883, is considered as the most essential and influential fractal, since it is a simple and perfect example for theory and applications of fractals. The idea of self-similarity received more attention in the work of Helge von Koch. He devised in 1904 a continuous but non-differentiable curve that never intersects itself. The curve is considered as one of the simplest regular fractals. Waclaw Sierpinski was one of the mathematicians who made significant contributions in the field of fractals. He introduced the famous triangular fractal in 1916, known as the Sierpinski gasket. The fractal is generated by a recursive process of removing symmetrical parts from an initial triangle. In an analogous way to the gasket, Sierpinski developed a square fractal known as the Sierpinski carpet. Julia sets gained significance in being generated using the dynamics of iterative function. They are discovered by Gaston Julia and Pierre Fatou in 1917-19, where they studied independently the iteration of rational functions in the complex plane [22]. During the same period, the mathematician Felix Hausdorff formulated the notion of fractional dimension which became a very important tool for studying and characterizing the geometrical complexity of fractals. Paul Lévy studied the self-similar curves and surfaces, and in 1938 he described a new fractal curve, the Lévy C curve. The field known today as the fractal geometry was developed by Mandelbrot during the last third of the twentieth century. He was one of the first to use computer to study and generate fractal shapes. In 1979, Mandelbrot visualized Julia sets including the most popular fractal called Mandelbrot set.

1.1.3 Relationship between Chaos and Fractals

Several researches pointed out that a close relationship between chaos and fractal geometry can be observed. This can be seen, for instant, in the dynamics of Fatou-Julia iteration used to construct Julia and Mandelbrot sets where two neighbor points in the domain which are close to the boundary may have completely different behavior.

That is, we can say about sensitivity in fractal structures. Chaos tells us about the state of irregularity and divergence of trajectories which depend in the nature of the dynamics, whereas the fractal concept can be used to study complex geometric structures. Therefore, the interlink between chaos and fractals is more clear when fractal dimension is used to measure the extent to which a trajectory fills its phase space. In other words, fractal dimension of the orbit in phase space implies the existence of a strange attractor [23]. The fundamental work on the chaotic nature of fractals has been done only for specific types categorized under the totally disconnected fractals [14, 24, 25]. In that work, the topological conjugacy concept was utilized to prove that these fractal sets are invariant for certain chaotic maps. Except for that, relatively few studies have been carried out on chaotic dynamical systems for fractals, and perhaps the most relevant one is what have been done on the Sierpinski carpet in [26]. In that research, the author shows that the dynamical system associated with a shift transformation defined on the Sierpinski carpet set is chaotic in the sense of topological mixing.

1.2 Replication of Chaos

It was shown in [27, 28] that chaotic behavior can be replicated through continuous-time systems. The idea is to consider chaos as an input for differential or hybrid equations. That is to insert chaos on the right-hand side of the equations and investigate the results of perturbation. Difference and differential equations are considered as the main sources of chaos in theory. This is why it is reasonable to consider the solutions of some systems of differential equations or discrete equations as inputs for the replication mechanism. These systems are called *generators* and the replication of chaos can be performed from a prior one to systems with large dimensions. The systems that receive the input and transmit chaos are called *replicators*. The replication mechanism can be constructed by taking into account a system of differential equations (the generator) which produces chaos, and using this system to influence in a unidirectional way, another system (the replicator) in such a manner that the replicator mimics the same ingredients of chaos provided to the generator.

For instance the generator can be considered as a system of the form

$$x' = f(t, x), \tag{11}$$

where $f : \mathbb{R} \times \mathbb{R}^m \to \mathbb{R}^m$ is a continuous function in all its arguments, and the replicator can be assumed to have the form

$$y' = Ay + g(x(t), y),$$

where $g : \mathbb{R}^m \times \mathbb{R}^n \to \mathbb{R}^n$ is a continuous function in all its arguments, the constant $n \times n$ real valued matrix A has real parts of eigenvalues all negative and the function $x(t)$ is a solution of system (11).

It is worthy of mention that the generator is not necessarily the element of the replication procedure since it can be replaced by another source of a chaotic input, and in applications it may be considered, for example, as chaotic inputs obtained from experimental activity.

The conception of replication of chaos is applied for different types of chaos such as Devaney's and Li-Yorke, where the extension of the formal properties and features of a complex motion can be observed in the dynamics of output such that the ingredients of these types of chaos are recognized. This is true for other appearances of chaos: intermittency, structure of the chaotic attractor, its fractal dimension, form of the bifurcation diagram, the spectra of Lyapunov exponents, etc. Replication of a known type of chaos can be extended to systems with arbitrary large dimension such that the replication between unidirectionally coupled systems results a system that admits the same type of chaos. The "morphogenesis" mechanism can be constructed by the formation of consecutive replications of chaos or replication of chaos from a core system. It is also possible to construct a result-system using these two mechanisms in a mixed style.

The technique of coupled systems is used in the study of synchronization of chaotic systems [29, 30]. The idea of chaos synchronization was first introduced by Pecora and Carroll [30]. Synchronization refers to the tendency to have the same dynamical behavior in coupled systems [31]. That is two or more chaotic systems adjust a given property of their motion to a common behavior [32]. The type of the chaos that the master and slave systems admit in the synchronization of chaotic systems, is

not taken into consideration during the analysis. However, in the process of replication of chaos, however, the type of chaos is kept invariant. That is why the classes which can be considered with respect to this invariance is expectedly wider then those investigated for synchronization of chaos [27, 28].

An interesting example of replication of chaos is the extension of unpredictability in Lorenz systems which has been introduced in [33]. In that paper, Lorenz systems are unidirectionally coupled such that the chaos expands from the drive system. The extension of sensitivity and period-doubling cascade are theoretically proved, and the appearance of cyclic chaos as well as intermittency in interconnected Lorenz systems are numerically demonstrated. The results are valid if the driving Lorenz system is chaotic and the response system is nonchaotic, but admits a global asymptotically stable equilibrium or a globally attracting limit cycle.

In the second chapter of this research, we apply the concept of replication of chaos to the sea surface temperature advection equations as well as low order ocean-atmosphere models. We utilize the results in unpredictable solutions of differential equations introduced in [19, 34] to prove that the solution of the advection equation admit chaos if its coefficients or its forced term is perturbed by a chaotic term. We investigate the extension of unpredictability of the sea surface temperature by applying the chaos extension mechanisms developed in [27] to coupled Vallis model and advection equations as regional models of ocean dynamics. Furthermore, we study the the possibility of the "vertical" extension of unpredictability between ocean and atmosphere by applying the Lorenz system for the atmosphere and the Vallis model for the ocean.

1.3 Dynamics through Fractal mappings

The famous Laplace's Demon is not only of strict physical determinism, but also related to the power of differential equations. When deterministically extended structures are taken into consideration, it is admissible that fractals are dense both in the nature and in the dynamics. In particular, this is true because fractal structures are closely related to chaos. This implies that dynamics have to be an instrument of the extension. Oppositely, one can animate the arguments for the Demon if dynamics

6

will be investigated with fractals. To make advances in the direction, first of all, one should consider fractals as states of dynamics. In other words, instead of single points and finite/infinite dimensional vectors, fractals should be points of trajectories as well as trajectories themselves. If one realizes this approach, fractals will be proved to be dense in the universe, since modeling the real world is based on differential equations and their developments. Our main goal is to initiate the involvement of fractals as states of dynamical systems, and in the first step we answer the simple question "How can fractals be mapped?". In the present study Julia sets and Sierpinski fractals are considered as initial points for the trajectories of the dynamics.

Fractals are in the forefront of researches in many areas of science as well as for interdisciplinary investigations [24, 35]. One cannot say that motion is a strange concept for fractals. Dynamics are beside the fractals immediately as they are constructed by iterations. It is mentioned in the book [36] that it is inadequate to talk about fractals while ignoring the dynamical processes which created them. That is, iterations are in the basis of any fractal, but we still cannot say that differential equations are widely interrelated to fractals, for instance, as much as manifolds [37]. Our present study is intended to open a gate for an inflow of methods of differential equations, discrete equations and any other methods of dynamics research to the realm of fractals. This will help not only to investigate fractals but also to make their diversity richer and ready for intensive applications. Formally speaking, in our investigation we join dynamics of iterations, which can be called inner dynamics, with outer dynamics of differential and discrete equations. The concept of fractals has already many applications, however, the range would be significantly enlarged if all the power of differential equations will be utilized for the structures. This is why our suggestions are crucial for fractals considered in biology, physics, city planning, economy, image recognition, artificial neural networks, brain activity study, chemistry, and all engineering disciplines [38, 39, 40, 41, 42, 43], i.e. in every place, where the geometrical objects in physical and/or abstract sense may appear [44]. It deserves to say that differential equations related to fractals were already discussed in [45, 46], where they are considered as domains of partial differential equations, but not as building blocks of trajectories. In this sense one can take advantage of the papers [45, 46] in the next development of our proposals. The same is true for the studies concerned with deep

analyses of fractals growth performed in [47, 48].

The most important fractals for our present study are Julia sets which were discovered in 1917-1918 by Julia and Fatou, both of whom independently studied the iteration of rational functions in the complex plane [22]. They established the fundamental results on the dynamics of complex functions published in their papers [44, 49]. In 1979, Mandelbrot visualized Julia sets. Although they are constructed depending on the dynamics of simple complex polynomials, the Mandelbrot set has a complicated boundary, and the Julia sets associated with points close to the boundary usually have amazing and beautiful structures. Julia and Mandelbrot fractals are very great achievements for set theory, topology, functions theory, chaos, and real world problems. Therefore, studies in the area has to be at the frontiers of modern sciences and applications. Additionally, the development of researches on the basis of fractals is of significant importance to any possible direction starting from the basis of set theory.

In our research, we make a possible study of mapping fractals, which is simple from one side since it relates to classical functions, but from another side it is a developed one since we apply the mapping function in a new manner, which nevertheless still relates to the original ideas of Julia. Based on the constructed mapping iteration, dynamics for fractals are introduced. We proceed upon the fact that motion of fractals comprehend as deformation was not considered in literature at all. From the mathematical point of view, the deformation is equivalent to mapping. Why mapping for fractals was not investigated in the literature before? The reason lies in the complexity of fractals building. Theoretically, the procedure is complex and sophisticated since it contains infinitely many steps. Consequently, to map fractals, one has to combine a map's algorithm with the complex algorithm of a fractal construction. We have found the combination, and it is one of the main achievements of the present study. That is, in fact, we introduce a new type of functions, with fractal domains, and determine the properties for the functions to have fractal-images and approve this. Moreover, using the algorithm of mapping, we find conditions for discrete equations to admit trajectories consisting of fractals as well as conditions for continuous trajectories of autonomous differential equations (dynamical systems) to be of fractals. Furthermore, a discussion about admitting fractal-points for non-autonomous differential equations is provided. For the theoretical discussions, we apply results

8

of the fractal geometry (dimension) and theorems and definitions from the theory of dynamical systems, differential and discrete equations theory.

CHAPTER 2

GLOBAL WEATHER AND CLIMATE IN THE LIGHT OF EL NIÑO-SOUTHERN OSCILLATION

2.1 Introduction and Preliminaries

The famous Lorenz equations give birth to the weather related observations. One of them is the unpredictability of weather in long period of time, which is a meteorological concept, and another one is that small changes of the climate and even weather at present may cause catastrophes for the human life in future. Issuing from this, we have taken into account the following three features of the Lorenz system, to emphasize the actuality of the present study. Firstly, it is a regional model. Secondly, for some values of its parameters the equations are non-chaotic. Finally, the model is of the atmosphere, but not of the hydrosphere. Therefore, one has to make additional investigations to reveal that the unpredictability of weather is a *global* phenomenon, and climatic catastrophes can be caused by physical processes at *any point* on the surface of the globe. The present research is concerned with all of the three factors issuing from the ocean surface dynamics of El Niño-Southern Oscillation type, and results of the former research [27, 33].

In this chapter, we study the chaotic behavior of hydrosphere and its influence on global weather and climate. We give mathematical arguments for the sea surface temperature (SST) to be unpredictable over the global ocean. The impact of SST variability on global climate is clear during global climate patterns, which involve large-scale ocean-atmosphere fluctuations similar to the El Niño-Southern Oscillation (ENSO). Sensitivity (unpredictability) is the core ingredient of chaos. Several researches suggested that the ENSO might be chaotic. It was Vallis [50, 51] who

revealed unpredictability of ENSO by reducing his model to the Lorenz equations. Interactions of ENSO and other global climate patterns may transmit chaos. We discuss the unpredictability as a global phenomenon through extension of chaos "horizontally" and "vertically" in coupled Vallis ENSO models, Lorenz systems, and advection equations by using theoretical as well as numerical analyses. To perform theoretical research, we apply the recent results on replication of chaos [27, 28] and unpredictable solutions of differential equations [19, 34], while for numerical analysis, we combine results on unpredictable solutions with numerical analysis of chaos in the advection equation.

2.1.1 Unpredictability of Weather and Deterministic Chaos

Global climate change has gained the attention of scientists and policymakers. The reason for that lies in its remarkable impact on human life on the Earth [52]. Climate change affects and controls many social, economic and political human activities. It was an essential motivation of human migration throughout history.

Weather is defined by the condition of the atmosphere at a specific place and time measured in terms of temperature, humidity, air pressure, wind, and precipitation, whereas climate can be viewed as the average of weather of a large area over a long period of time [53]. Some definitions of climate expand to include the conditions of not only the atmosphere, but also the rest components of the climate system: hydrosphere, cryosphere, lithosphere, biosphere, and, according to Vernadsky, noösphere [54].

During the last few decades, big efforts have been made to develop weather and climate change forecasting models. Due to the chaotic nature of weather, the forecasting range of weather prediction models is limited to only a few days. Climate models are more complicated than ordinary weather forecasting models, since they need to include additional factors of climate system that are not important in the weather forecast [55]. Understanding the concepts of chaos is an important step toward better comprehension of the natural variability of the climate system on different time scales. This involves determining what the reasons and sources that stand behind of presence of chaos in weather and climate models. Any progress made in this path will

be helpful to adjust the conception of climate change and find solutions for climate control.

Chaos can be defined as aperiodic long-term behavior in a deterministic system that exhibits sensitive dependence on initial conditions [4]. Predictability consists of constructing a relationship between cause and effect by which we can predict and estimate the future behavior of a physical property. Unpredictability means the failure of such empirical or theoretical relationships to predict due to consisting of noise term(s), mathematical nature of the relationships or intrinsic irregularity of the physical property itself. Mathematically unpredictability is considered as a result of the sensitive dependence on initial conditions, which is an essential feature of Devaney chaos [14]. Recently, it is theoretically proved that a special kind of Poisson stable trajectory, called an unpredictable trajectory, gives rise to the existence of Poincaré chaos [18, 19, 56].

Unpredictability in the dynamics of weather forecast models was firstly observed by E. N. Lorenz. He developed a heat convection model consisting of twelve equations describing the relationship between weather variables such as temperature and pressure. Lorenz surprisingly found that his system was extremely sensitive to initial conditions. Later, in his famous paper [13], he simplified another heat convection model to a three-equation model that has the same sensitivity property [57]. This model is defined by the following nonlinear system of ordinary differential equations:

$$
\begin{aligned}
\frac{dx}{dt} &= -\sigma\,x + \sigma y, \\
\frac{dy}{dt} &= r\,x - xz - y, \\
\frac{dz}{dt} &= xy - b\,z,
\end{aligned}
\tag{21}
$$

where the variable x represents the velocity of the convection motion, the variable y is proportional to the temperature difference between the ascending and descending currents, and the variable z is proportional to the deviation of the vertical temperature profile from linearity, whereas the constants σ, r, and b are positive physical parameters. Model (21) describes the thermal convection of a fluid heated from below between two layers. With certain values of these parameters, Lorenz system possesses intrinsic chaos and produces the so-called Lorenz butterfly attractor.

13

The dynamical nature of weather and climate requires a deeper understanding of the interaction and feedback mechanisms between the climate system components as well as the individual one between different regions of a certain component. To study the behavior of one component of the climate system at a specific region, a single model defined on a particular spatial and temporal scales is acceptable and the accuracy of the outputs mainly depends on the number of climate variables and parameters included in the model. Due to the inevitable simplifications usually adopted for the construction of such models, the outputs include potential errors even for limited time scale. Super-modeling is a recently proposed technique has been applied to reduce model error and improve prediction. The strategy is based on inter-connection of different climate models that synchronize on a common solution, referred to as the supermodel solution [58, 59, 60]. Here, the synchronization in connected models plays an important role for compensating errors in order to achieve an optimal prediction. In this research, different models represent the dynamics of neighbor regions in the same component and different components of the climate system are coupled to investigate the global role of chaos in weather and climate through the inter-ocean and ocean-atmosphere interactions. The paper [33] was concerned with the extension of chaos through Lorenz systems. It was demonstrated in [33] that Lorenz systems can be unidirectionally coupled such that the drive system influences the response system, which is non-chaotic in the absence of driving, in such a way that the latter also possesses chaos. Additionally, it was showed that the synchronization does not take place in the dynamics of this types of coupled system. A possible connection of these results to the global weather dynamics was also provided in that study.

2.1.2   Ocean-Atmosphere Interaction and its Effects on Global Weather

Coupled ocean-atmosphere models are the most fundamental tool for understanding the natural processes that affect climate. These models have been widely applied to interpret and predict global climate phenomena such as ENSO [61]. In meteorology and climate science, SST is considered as a very important factor in ocean-atmosphere interaction, where it plays a basic role in determining the magnitude and direction of the current velocity, as well as the ocean surface wind speed. It is difficult to give a precise definition of SST due to the complexity of the heat transfer operations

in the mixed layer of upper ocean. In general, however, it can be defined as the bulk temperature of the oceanic mixed layer with a depth varies from $1\,m$ to $20\,m$ depending on the measurement method used [62]. The importance of SST stems from the fact that the world's oceans cover over $70\,\%$ of the whole surface of the globe. This large contact area gives way to an active ocean-atmosphere interaction and sometimes becomes a fertile place for complex feedbacks between the ocean and atmosphere that drive an irregular climate change.

The most important example of the interactions and feedbacks between the ocean and the atmosphere is El Niño and Southern Oscillation (ENSO) which is defined as a global coupled ocean-atmosphere phenomenon occurs irregularly in the Pacific Ocean about every 2 to 7 years [63]. This phenomenon is accompanied by undesirable changes in weather across the tropical Pacific and losses in agricultural and fishing industries especially in South America. The El Niño mechanism can be briefly summarized as follows: During normal conditions in the equatorial Pacific, trade winds blow from east to west driving the warm surface current in the same direction. As a consequence of this, warm water accumulates in the western Pacific around southeast Asia and northern Australia. On the opposite side of the ocean around central and south America, the warm water, pushed to the west, is replaced by upwelling cold deep water. During El Niño conditions, the trade winds are much weaker than normal. Because of this and due to SST difference, warm water flows back towards the western Pacific. This situation involves large changes in air pressure and rainfall patterns in the tropical Pacific. The cool phase of this phenomenon is called La Nina, which is an intensification of the normal situation. The term "Southern Oscillation" is usually used to refer to the difference of the sea-level pressure (SLP) between Tahiti and Darwin, Australia. Bjerknes [64] conclude that El Niño and the Southern Oscillation are merely two different results of the same phenomenon. These phases of the phenomenon are scientifically called El Niño Southern Oscillation or shortly ENSO. From the above mechanism we can note that the ENSO dynamics is a perfect example of self-excited oscillating systems.

The ramifications of El Niño are not restricted to the Pacific basin alone, but have widespread effects which severely disrupt global weather patterns. In the last few decades scientists developed theories about the climatic engine which produced El

Niño, and they are trying to explain how that engine interact with the great machine of global climate. Although remarkable progress has been made in monitoring and forecasting the onset of El Niño, it is still challenging to predict its intensity and the impact of the event on global weather. Study of ENSO is considered as a key to understanding climate change, it is a significant stride toward the meteorology's ultimate goal, "accurate prediction and control of world weather".

Besides the ENSO, there are several other atmospheric patterns that occur in different regions of the Earth. These phenomena are interacting in very complicated ways. Many researchers paid attention to the mutual influence of these phenomena and investigated if there is any co-occurrence relationship or interaction between them.

The most similar atmosphere-ocean coupled phenomenon to ENSO is the Indian Ocean Dipole (IOD), which occur in the tropical Indian Ocean, and it is sometimes called the Indian Niño. IOD has normal (neutral), negative and positive phases. During neutral phase, Pacific warm water, driven by the Pacific trade winds, cross between south Asia and Australia and flow toward the Indian Ocean. Because of the westerly wind, the warm water accumulates in the eastern basin of Indian Ocean. In the negative IOD phase with the coincidence of strength of the westerly wind, warmer water concentrate near Indonesia and Australia, and cause a heavy rainfall weather in these regions and cooler SST and droughts in the opposite side of the Indian Ocean basin around the eastern coast of Africa. The positive phase is the reversal mode of the negative phase, i.e., what happened in the east side will happen in west side and vice versa.

From the above we can see that there is a symmetry between the IOD and ENSO mechanisms. Indeed, SST data shows that the Indian Ocean warming appears as a near mirror image of ENSO in the Pacific [65]. In addition, the IOD is likely to have a link with ENSO events, where a positive (negative) IOD often occurs during El Niño (La Nina) [66, 67]. Luo et al. [68] investigated the ENSO-IOD interactions, and they suggest that IOD may significantly enhance ENSO and its onset forecast, and vice versa. Several other researchers like [69, 70] studied the relationship and interaction between ENSO and IOD. It should be noted here that (as in all these studies) the SST considered as the major variable, indicator and index for these events.

16
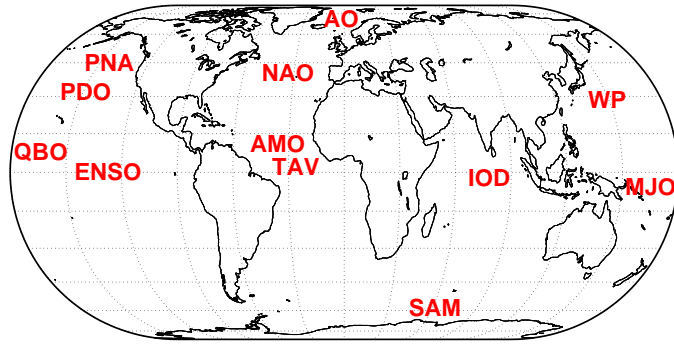
Figure 2.1: The major global climate patterns

Other important atmosphere-ocean coupled phenomena like Pacific Decadal Oscillation (PDO), Atlantic Multidecadal Oscillation (AMO), Southern Annular Mode (SAM), Tropical Atlantic Variability (TAV), North Atlantic Oscillation (NAO), Arctic Oscillation/Northern Annular Mode (AO/NAM), Madden-Julian Oscillation (MJO), Pacific/North American pattern (PNA), Quasi-Biennial Oscillation (QBO), and Western Pacific pattern (WP) have significant influences on weather and climate variability throughout the world. Similar to the relationship between ENSO and IOD, various studies show expected relationships between these phenomena and mutual effects on their predictability. Figure 2.1 shows the places of occurrence of the major atmospheric patterns and Table 2.1 gives brief descriptions of them [71, 72, 73]. These pattern modes have different degrees of effect on SST. In Table 2.1 we see that the patterns that remarkably influence the ocean temperature are indexed by SST, whereas those that are most correlated with air pressure, the main indexes of them are based on SLP.

2.1.3 El Niño Chaotic Dynamics

The SST behavior associated with ENSO indicates irregular fluctuations. The ENSO indicator NINO3.4 index, for example, is one of the most commonly used indices, where the SST anomaly averaged over the region bounded by $5°N–5°S$, $170°–120°W$ [74]. Figure 2.2 shows the oscillatory behavior of SST in the NINO3.4 region. Data from the Hadley Centre Sea-Ice and SST dataset HadISST1 [75] is used to generate

17

Term	Descriptions	Main Index	Timescale
ENSO	An irregularly periodical variation in sea surface temperatures over the tropical eastern Pacific Ocean	SST	3–7 years
QBO	An oscillation of the equatorial zonal wind in the tropical stratosphere	SLP	26–30 months
PDO	A low-frequency pattern similar to ENSO occurs primarily in the Northeast Pacific near North America	SST	20–30 years
PNA	An atmospheric pressure pattern driven by the relationship between the warm ocean water near Hawaii and the cool one near the Aleutian Islands of Alaska	SLP	7–8 days
AO/NAM	Defined by westerly winds changes driven by temperature contrasts between the tropics and northern polar areas	SLP	1–9 months
NAO	Large scale of pressure varies in opposite directions in the North Atlantic near Iceland in the north and the Azores in the south	SLP	9–10 days
TAV	Like ENSO, but it exhibits a north-south low frequency oscillation of the SST gradient across the equatorial Atlantic Ocean	SST	10–15 years
AMO	A mode of natural variability occurring in the North Atlantic Ocean and affects the SST on different modes on multidecadal timescales	SST	55–80 years
SAM	Defined by westerly winds changes driven by temperature contrasts between the tropics and southern polar areas	SLP	30–70 days
IOD	An irregular oscillation of sea-surface temperatures in equatorial areas of the Indian Ocean	SST	2–5 years
WP	A low-frequency variability characterized by north-south dipolar anomalies in pressure over the Far East and western North Pacific	SLP	7–8 days
MJO	An equatorial traveling pattern of anomalous rainfall Located in the tropical Pacific and Indian oceans	SLP	40–50 days

Table 2.1: The major climate variability systems
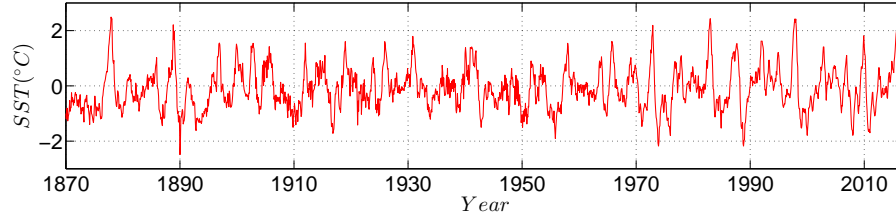
Figure 2.2: Sea surface temperature anomalies of NINO3.4 region. The data utilized in the figure is from the Hadley Centre Sea-Ice and SST dataset HadISST1.

the figure. This behavior encourages many scientists to answer the question: Is ENSO a self-sustained chaotic oscillation or a damped one, requiring external stochastic forcing to be excited? [76]. There are different hypotheses for the source of chaos in ENSO. According to Neelin and Latif [77], deterministic chaos within the nonlinear dynamics of coupled system, uncoupled atmospheric weather noise and secular variation in the climatic state are the possible source of ENSO irregularity. Tiperman et al. [78] concluded that the chaotic behavior of ENSO is caused by the irregular jumping of the ocean-atmosphere system among different nonlinear resonances. Several studies like [79, 80] support this assumption and attributed the irregularity and the unpredictability of ENSO to influence of stochastic forcing generated by weather noise. Other studies like [81, 82] infer that ENSO is intrinsically chaotic, which means that the irregularity and the loss of predictability are independent of the chaotic nature of weather.

Practically, investigating chaos in ENSO needs long time-series of data, which make the task quite difficult experimentally. Vallis [50, 51], developed a conceptual model of ENSO and suggested that the ENSO oscillation exhibits a chaotic behavior. Vallis used finite difference formulation to reduce two dimensional versions of advection and continuity equations to a set of ordinary differential equations. In addition, he assumed that the zonal current is driven by the surface wind, which is in turn proportional to the temperature difference across the ocean. The model is described by the

19

set of equations

$$
\begin{aligned}
\frac{du}{dt} &= \beta \left(T_e - T_w \right) - \lambda \left(u - u^* \right), \\
\frac{dT_w}{dt} &= \frac{u}{2\Delta x} \left(\bar{T} - T_e \right) - \alpha \left(T_w - T^* \right), \\
\frac{dT_e}{dt} &= \frac{u}{2\Delta x} \left(T_w - \bar{T} \right) - \alpha \left(T_e - T^* \right),
\end{aligned}
\tag{22}
$$

where u represents the zonal velocity, T_w and T_e are the SST in the western and eastern ocean respectively, $\bar{T}$ is the deep ocean temperature, T^* is the steady state temperature of ocean, u^* represents the effect of the mean trade winds, Δx is the width of the ocean basin, and α, β and λ are constants.

By nondimensionalizing Equations (22) and forming the sum and difference of the two temperature equations, one can see that these equations have the same structure as the Lorenz system (21). Vallis utilized the fact that the Lorenz system, with specific parameters, is intrinsically chaotic, and showed that a chaotic behavior of the sum and difference of the west and east SST can be obtained.

ENSO, as mentioned above, occurs as a result of the interaction of the ocean and atmosphere. Therefore, modeling of ENSO would be a good instrument to research unpredictability not only in the atmosphere but also in the hydrosphere. Nevertheless, ENSO provides the arguments that unpredictability is also proper for sea water parameters which possibly can be reduced to a single one, the SST, if one excludes flow characteristics. Vallis saved in the model only hydrosphere variables ignoring the variation of atmosphere parameters when he considers chaos problem. In our opinion, however, the model is appreciated as a pioneer one, and furthermore, it implies chaos presence in the Pacific ocean water. Hopefully, in the future, ENSO with both atmosphere and hydrosphere characteristics being variable will be modeled, but this time we focus on chaotic effects of ENSO by utilizing the Vallis model.

2.1.4 Sea Surface Temperature Advection Equation

The temporal and spatial evolution of the SST is governed by a first order quasi-linear partial differential equation, the advection equation. If we denote the SST by T, the temperature advection equation of mixed layer of fixed depth can be written in the

form [83, 84]

$$\frac{\partial T}{\partial t} + u\frac{\partial T}{\partial x} + v\frac{\partial T}{\partial y} + w\frac{\partial T}{\partial z} = f(t, x, y, z, T), \tag{23}$$

where u, v, w are the zonal, meridional and vertical components of current velocity, respectively. These velocities theoretically must satisfy the continuity equation

$$\frac{\partial}{\partial x}(\rho u) + \frac{\partial}{\partial y}(\rho v) + \frac{\partial}{\partial z}(\rho w) = -\frac{\partial \rho}{\partial t}, \tag{24}$$

where ρ is the seawater density.

The inhomogeneous (forcing) term f on the right-hand side of Equation (23) consists of the shortwave flux, the evaporative heat flux, the combined long-wave back-radiation and sensible heat flux and heat flux due to vertical mixing [85]. This term can be described by [86, 87, 88]

$$f \approx \frac{1}{h\rho\, C_p}\frac{\partial q}{\partial z} + D, \tag{25}$$

where h is the mixed layer depth, C_p is the heat capacity of seawater, q is radiative and diffusive heat flux, and D is the thermal damping (the numerical diffusion operator).

The spatial and temporal domain of Equation (23) depend on the region and the nature of the phenomenon under study. For studying ENSO or IOD, for instance, there are various regions for monitoring SST. NINO3.4 is one of the most commonly used indices for ENSO. Dipole Mode Index (DMI) is usually used for IOD, and it depends on the difference in average SST anomalies between the western 50°E–70°E, 10°N–10°S and the eastern 90°E–110°E, 0°–10°S boxes [89]. The mixed layer depth h varies with season and depends on the vertical heat flux through the upper layers of the ocean. The average of mixed layer depth is about $30\,\text{m}$ [90]. Different studies of ocean-atmosphere coupled models considered different regions of various sizes. Zebiak and Cane [81], for example, developed a model of ENSO. They considered a rectangular model extending from 124°E to 80°W and 29°N to 29°S, with constant mixed layer depth of $50\,\text{m}$ and 90 years simulation.

From the above we find that the domain of Equation (23) depends on the purpose of the study. To study ENSO, for instance, we would cover a big region of pacific ocean basin, and if we choose the origin of coordinates to be at 160°E on the Equator, we can write the domain of (23) as follows

$$t \geq 0, \quad 0 \leq x \leq 9000\,\text{km}, \quad -3000\,\text{km} \leq y \leq 3000\,\text{km}, \quad -100\,\text{m} \leq z \leq 0.$$

The inhomogeneous term in Equation (23), which includes mixing processes of heat transfer, plays the main role for chaotic dynamics. In addition to this term, a chaotic behavior in ocean current velocity terms may also produce an unpredictable behavior in SST. These causes of unpredictability are proved analytically and numerically by perturbing these terms by unpredictable functions. In this study we treat Equation (23) mathematically without paying attention to the dimensions of the physical quantities. The important thing to us is the possibility of presence of chaos in this advection equation endogenously or be acquired from other equation or system. The advection equation, in addition to the Vallis model and the Lorenz system, will be used to demonstrate the extension of unpredictability "horizontally" through the global ocean and "vertically" between ocean and atmosphere.

2.1.5 Unpredictability and Poincaré Chaos

There are different types and definitions of chaos. Devaney [14] and Li-Yorke [1] chaos are the most frequently used types, which are characterized by transitivity, sensitivity, frequent separation and proximality. Another common type is the period-doubling cascade, which is a sort of route to chaos through local bifurcation [15, 16, 17]. In the papers [18, 19], Poincaré chaos was developed by introducing the theory of unpredictable point and unpredictable function, which are built on the concepts of Poisson stable point and function. We define unpredictable point as follows. Let (X, d) be a metric space and $\pi : \mathbb{T} \times X \to X$ be a flow on X, where $\mathbb{T}$ refer to either the set of real numbers or the set of integers. We assume that the triple (π, X, d) defines a dynamical system.

Definition 1. *[18] A point $p \in X$ and the trajectory through it are unpredictable if there exist a positive number ϵ (the unpredictability constant) and sequences $\{t_n\}$, $\{\tau_n\}$ both of which diverge to infinity such that $\lim_{n \to \infty} \pi(t_n, p) = p$ and $d[\pi(t_n + \tau_n, p), \pi(\tau_n, p)] \geq \epsilon$ for each $n \in \mathbb{N}$.*

Definition 1 describes unpredictability as individual sensitivity for a motion, i.e., it is formulated for a single trajectory. The Poincaré chaos is distinguished by Poisson stable motions instead of periodic ones. Existence of infinitely many unpredictable Poisson stable trajectories that lie in a compact set meet all requirements of chaos.

Based on this, chaos can be appeared in the dynamics on the quasi-minimal set which is the closure of a Poisson stable trajectory. Therefore, the Poincaré chaos is referred to as the dynamics on the quasi-minimal set of trajectory initiated from unpredictable point.

The definition of an unpredictable function is as follows.

Definition 2. *[34] A uniformly continuous and bounded function $\varphi : \mathbb{R} \to \mathbb{R}^m$ is unpredictable if there exist positive numbers ϵ, δ and sequences $\{t_n\}$, $\{\tau_n\}$ both of which diverge to infinity such that $\|\varphi(t + t_n) - \varphi(t)\| \to 0$ as $n \to \infty$ uniformly on compact subsets of $\mathbb{R}$, and $\|\varphi(t + t_n) - \varphi(t)\| \geq \epsilon$ for each $t \in [\tau_n - \delta, \tau_n + \delta]$ and $n \in \mathbb{N}$.*

To determine unpredictable functions, we apply the uniform convergence topology on compact subsets of the real axis. This topology allows us to construct Bebutov dynamical system on the set of the bounded functions [56, 91]. Consequently, the unpredictable functions imply presence of the Poincaré chaos.

2.1.6 The Role of Chaos in Global Weather and Climate

The topic of weather and climate is one of the most profoundly important issues concerning the international community. It becomes very actual since the catastrophic phenomena such as global warming, hurricanes, droughts, and floods. This is why weather and climate are agenda of researches in physics, geography, meteorology, oceanography, hydrodynamics, aerodynamics and other fields. The problem is global, that is a comprehensive model would include the interactions of all major climate system components, howsoever, for a specific aspect of the problem, a appropriate model combination can be considered [92]. In the second half of the last century, it was learned [13] that the weather dynamics is irregular and sensitive to initial conditions. Thus the chaos was considered as a characteristic of weather which can not be ignored. Moreover, chaos can be controlled [93, 94]. These all make us optimistic that the researches of weather and climate considering chaos effect may be useful not only for the deep comprehension of their processes but also for control of them. In the research [27], we have shown how a local control of chaos can be expanded globally.

It is not wrong to say that in meteorological studies, chaos is considered as a severe limiting factor in the ability to predict weather events accurately [95]. Beside this one can say that chaos is also a responsible factor for climate change if it is considered as a weather consequence. This is true, firstly, because of the weather unpredictability, since predictability can be considered as a useful feature of climate with respect to living conditions, and secondly, as the small weather change may cause a global climate change in time. Accordingly, it is possible to say that the control of weather, even a limited artificial one, bring us to a change of climate.

The chaotic behavior has also been observed in several models of ENSO [77]. Presence of chaos in the dynamic of this climate event provides other evidence of the unpredictable nature of the global weather. Besides the Lorenz chaos of atmosphere, "Vallis chaos" takes place in the hydrosphere. Without exaggerating, we can say that chaos seems to be inherent at the essence of any deterministic climate model. Therefore, unpredictability can be globally widespread phenomenon through constructive interactions between the components of the climate system.

To give a sketch how chaos is related globally to weather and climate, we will use, in the present research, information on dynamics of ENSO which will mainly utilize the Vallis model as will as the SST advection equation and the Lorenz equations. They will be properly coupled to have the global effect. It is apparent that, in the next research, the models will possibly be replaced by more developed ones, but our main idea is to demonstrate a feasible approach to the problem by constructing a special net of differential equations system. Obviously, one can consider the net as an instrument which can be subdued to an improvement by arranging new perturbation connections.

Proceeding from aforementioned remarks and as a part of the scientific work, we focus on one possible aspect of global weather and climate dynamics based on El Niño phenomenon. To address this aim, we first review the Vallis model research for El Niño in Subsection 2.1.3, then, in Section 2.2 we analyze the presence of chaos in isolated models for the SST advection equation. In Section 2.3, the extension of chaos in hydrosphere discussed through coupling of advection equation, the Vallis model and also mixing advection equation with the Vallis model. In paper [33] chaos as a global phenomenon in atmosphere was considered, but it is clear that, to say

about the globe weather one should take into account hydrosphere as well as the interaction processes between atmosphere and seas. For this reason Section 2.4 is written where chaos extension from ocean to air and vice versa is discussed on the base of the Lorenz and Vallis models. So, finalizing the introduction we can conclude that the present chapter is considered as an attempt to give a sketch of the global effects of chaos on weather and climate. This results are supposed to be useful for geographers, oceanographers, climate researchers and those mathematician who are looking for chaotic models and theoretical aspects of chaos researching.

2.2 Unpredictable Solution of the Advection Equation

In this section we study the presence of Poincaré chaos in the dynamics of Equation (23). We expect that the behavior of the solutions of (23) depends on the function f and the current velocity components u, v, w, which are used in the equation. From Equation (25), we see that the forcing term f depends mainly on the heat fluxes between the sea surface and atmosphere which is governed by SST, air temperature and wind speed, as well as between layers of sea which is caused by sea temperature gradient and vertical (entrainment) velocity. Therefore, this forcing term can be a natural source of noise and irregularity. Ocean currents are mainly driven by wind forces, as well as temperature and salinity differences [96]. Thence again we can deduce that the irregular fluctuations of wind may be reflected in the behavior of SST.

To demonstrate the role of the function f in the dynamics of Equation (23), let us take into account the equation

$$\frac{\partial T}{\partial t} + u\frac{\partial T}{\partial x} + v\frac{\partial T}{\partial y} + w\frac{\partial T}{\partial z} = -0.7\,T + 0.3\,w_1\,T + 5\,\sin(xt), \qquad (26)$$

where the current velocity components are defined by $u = \sin(\frac{x}{2}) + \sin(t) + 3$, $v = -0.02$, and $w = -\frac{1}{2}\cos(\frac{x}{2})z$.

Figure 2.3 represents the solution of (26) corresponding to the initial data $T(0,0,0,0) = 0.5$. It is seen in Figure 2.3 that the solution of Equation (26) has an irregular oscillating behavior, whereas in the absence of the term $5\sin(xt)$ in the function f, the solution approaches the steady state. Even though the behavior of this numerical solution depends on the step size of the numerical scheme used, this situation leads us
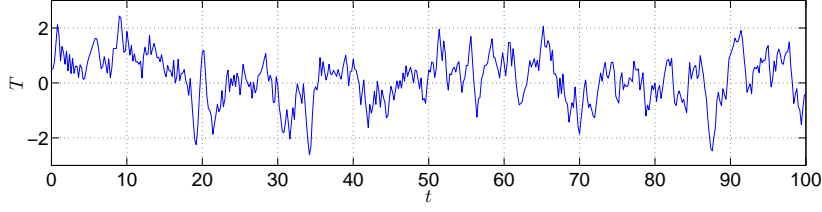
Figure 2.3: The solution of Equation (26) with the initial condition $T(0, 0, 0, 0) = 0.5$. The figure shows that the forcing term f has a significant role in the dynamics of (23).

to consider that the forcing term f has a dominant role in the behavior of SST.

To investigate the existence of an unpredictable solution in the dynamics of Equation (23) theoretically, let us apply the method of characteristics. If we parametrize the characteristics by the variable t and suppose that the initial condition is given by $T(t_0, x, y, z) = \Phi(x, y, z)$, where t_0 is the initial time, then we obtain the system

$$
\begin{aligned}
\frac{dx}{dt} &= u(t, x, y, z, T), \\
\frac{dy}{dt} &= v(t, x, y, z, T), \\
\frac{dz}{dt} &= w(t, x, y, z, T), \\
\frac{dT}{dt} &= f(t, x, y, z, T),
\end{aligned}
\tag{27}
$$

with the initial conditions

$$
x(t_0) = x_0, \quad y(t_0) = y_0, \quad z(t_0) = z_0, \quad T(t_0, x_0, y_0, z_0) = \Phi(x_0, y_0, z_0).
$$

In system (27), we assume that u, v, w, and f are functions of x, y, z, t, and T, and they have the forms

$$
\begin{aligned}
u &= a_1 x + a_2 y + a_3 z + a_4 T + U(x, y, z, T), \\
v &= b_1 x + b_2 y + b_3 z + b_4 T + V(x, y, z, T), \\
w &= c_1 x + c_2 y + c_3 z + c_4 T + W(x, y, z, T), \\
f &= d_1 x + d_2 y + d_3 z + d_4 T + F(x, y, z, T),
\end{aligned}
\tag{28}
$$

where a_i, b_i, c_i, d_i, $i = 1, 2, 3, 4$, are real constants and the functions U, V, W, F are

26

continuous in all their arguments. System (27) can be expressed in the form

$$X'(t) = AX(t) + Q(t), \tag{29}$$

in which

$$X(t) = \begin{bmatrix} x \\ y \\ z \\ T \end{bmatrix}, \qquad A = \begin{bmatrix} a_1 & a_2 & a_3 & a_4 \\ b_1 & b_2 & b_3 & b_4 \\ c_1 & c_2 & c_3 & c_4 \\ d_1 & d_2 & d_3 & d_4 \end{bmatrix}, \qquad Q = \begin{bmatrix} U \\ V \\ W \\ F \end{bmatrix}. \tag{210}$$

The following theorem is needed to verify the existence of Poincaré chaos in the dynamics of Equation (23).

Theorem 1. *[19] Consider the system of ordinary differential equations*

$$X'(t) = A\,X(t) + G(X(t)) + H(t), \tag{211}$$

where the $n \times n$ constant matrix A has eigenvalues all with negative real parts, the function $G : \mathbb{R}^n \to \mathbb{R}^n$ is Lipschitzian with a sufficiently small Lipschitz constant, and $H : \mathbb{R} \to \mathbb{R}^n$ is a uniformly continuous and bounded function. If the function $H(t)$ is unpredictable, then system (211) possesses a unique uniformly exponentially stable unpredictable solution, which is uniformly continuous and bounded on the real axis.

In the remaining parts of the present section, we will discuss the unpredictability when SST is chaotified by external irregularity. For that purpose let us consider the logistic map

$$\eta_{j+1} = 3.91\,\eta_j\,(1 - \eta_j),\ j \in \mathbb{Z}. \tag{212}$$

According to Theorem 4.1 in [19], the map (212) is Poincaré chaotic such that it possesses an unpredictable trajectory.

Next, we define a function $\phi(t)$ by

$$\phi(t) = \int_{-\infty}^{t} e^{-2(t-s)}\gamma^*(s)\,ds, \tag{213}$$

27

where

$$\gamma^*(t) = \begin{cases} 1.5, & \zeta_{2j}^* < t \le \zeta_{2j+1}^*, \quad j \in \mathbb{Z}, \\ 0.3, & \zeta_{2j-1}^* < t \le \zeta_{2j}^*, \quad j \in \mathbb{Z}, \end{cases} \tag{214}$$

is a relay function. In (214), the sequence $\{\zeta_j^*\}$ of switching moments is generated through the equation $\zeta_j^* = j + \eta_j^*, \ j \in \mathbb{Z}$, where $\{\eta_j^*\}$ is an unpredictable trajectory of the logistic map (212).

One can confirm that $\phi(t)$ is bounded such that $\sup_{t \in \mathbb{R}} |\phi(t)| \le 3/4$. It was shown in paper [19] that the function $\phi(t)$ is the unique uniformly exponentially stable unpredictable solution of the differential equation

$$\vartheta'(t) = -2\vartheta(t) + \gamma^*(t). \tag{215}$$

It is not an easy task to visualize the unpredictable function $\phi(t)$. Therefore, in order to illustrate the chaotic dynamics, we take into account the differential equation

$$\vartheta'(t) = -2\vartheta(t) + \gamma(t), \tag{216}$$

where

$$\gamma(t) = \begin{cases} 1.5, & \zeta_{2j} < t \le \zeta_{2j+1}, \quad j \in \mathbb{Z}, \\ 0.3, & \zeta_{2j-1} < t \le \zeta_{2j}, \quad j \in \mathbb{Z}, \end{cases} \tag{217}$$

and the sequence $\{\zeta_j\}$ satisfies the equation $\zeta_j = j + \eta_j, \ j \in \mathbb{Z}$, in which $\{\eta_j\}$ is a solution of (212) with $\eta_0 = 0.4$. The coefficient 3.91 used in the logistic map (212) and the initial data $\eta_0 = 0.4$ were considered for shadowing analysis in the paper [97].

We depict in Figure 2.4 the solution of Equation (216) with $\vartheta(0) = 0.3$. It is seen in Figure 2.4 that the behavior of the solution is irregular, and this support that the function $\phi(t)$ is unpredictable.
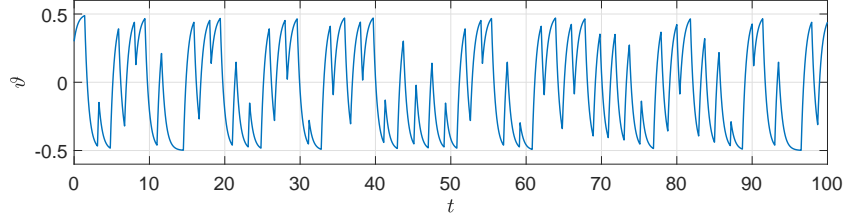
28

Figure 2.4: The solution of Equation (216) with $\vartheta(0) = 0.3$. The figure support that the function $\phi(t)$ is unpredictable.

2.2.1 Unpredictability Due to the Forcing Source Term

Let us perturb Equation (23) with the unpredictable function $\phi(t)$ defined by (213) and set up the equation

$$\frac{\partial T}{\partial t} + u\frac{\partial T}{\partial x} + v\frac{\partial T}{\partial y} + w\frac{\partial T}{\partial z} = f(t, x, y, z, T) + \psi(\phi(t)), \qquad (218)$$

where u, v, w, and f are in the form of (28) and $\psi : [-3/4, 3/4] \to \mathbb{R}$ is a continuous function.

Using the method of characteristics, one can reduce Equation (218) to system (27) that can be expressed in the form of (211) with

$$G(X(t)) = \begin{bmatrix} U \\ V \\ W \\ F \end{bmatrix}, \qquad H(t) = \begin{bmatrix} 0 \\ 0 \\ 0 \\ \psi(\phi(t)) \end{bmatrix}.$$

According to the result of Theorem 5.2 in [19], if there exist positive constants L_1 and L_2 such that

$$L_1 |s_1 - s_2| \leq |\psi(s_1) - \psi(s_2)| \leq L_2 |s_1 - s_2| \qquad (219)$$

for all $s_1, s_2 \in [-3/4, 3/4]$, then the function $H(t)$ is also unpredictable.

Now, in Equation (218), let us take $u = -0.03x + 0.1\sin(\frac{x}{80}) + 0.4$, $v = -0.01y - 0.05\sin(y)$, $w = -0.02z + (0.05\cos(y) - 0.00125\cos(\frac{x}{80}))z$, $\psi(s) = 6s$, and $f(t, x, y, z, T) = -1.5T + 0.1w_2 T$. Since the conditions of Theorem 1 are valid and inequality (219) holds for these choices of ψ, f, u, v, and w, Equation (218) exhibits Poincaré chaos.
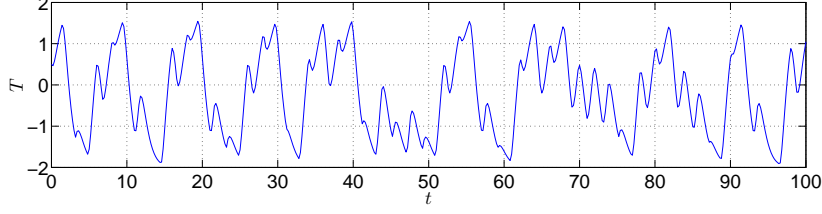
29

Figure 2.5: The solution of Equation (220) with the initial condition $T(0, 0, 0, 0) = 0.5$. The figure reveals the presence of an unpredictable solution in the dynamics of (218).

In order to simulate the chaotic behavior, we consider the equation

$$\frac{\partial T}{\partial t} + u\frac{\partial T}{\partial x} + v\frac{\partial T}{\partial y} + w\frac{\partial T}{\partial z} = f(t, x, y, z, T) + \psi(\vartheta(t)), \qquad (220)$$

where $\vartheta(t)$ is the function depicted in Figure 2.4, and u, v, w, f, ψ are the same as above. Figure 2.5 shows the solution $T(t, x, y, z)$ of (220) corresponding to the initial condition $T(0, 0, 0, 0) = 0.5$. It is seen in Figure 2.5 that the behavior of the solution is chaotic, and this supports the result of Theorem 1 such that Equation (218) admits an unpredictable solution.

Next, we will visualize the chaotic dynamics in the integral surface of SST. For that purpose, we omit the term of the meridional advection $v\frac{\partial T}{\partial y}$ in (218), which has less effect on SST compared with the zonal and vertical advections [98], and set up the equation

$$\frac{\partial T}{\partial t} + u\frac{\partial T}{\partial x} + w\frac{\partial T}{\partial z} = -1.5\,T + w\,T + 6\,\vartheta(t), \qquad (221)$$

where $u = 1.2 + 0.1\sin(\frac{x}{80}) + 0.05\sin(3t)$ and $w = 0.1 - 0.00125\cos(\frac{x}{80})z$. In (221), $\vartheta(t)$ is again the function shown in Figure 2.4.

We apply a finite difference scheme to solve Equation (221) directly. In such a scheme, we need to specify boundary conditions along with an initial condition. Using the initial condition $T(0, x, z) = 5$ and the boundary conditions $T(t, 0, z) = T(t, x, 0) = 0.5$, we represent in Figure 2.6 the integral surface of (221) with respect to t, x, and the fixed value $z = 0$ for $5 \leq x \leq 20$ and $0 \leq t \leq 100$. Figure 2.6 supports the result of Theorem 1 one more time such that Poincaré chaos is present in the dynamics.
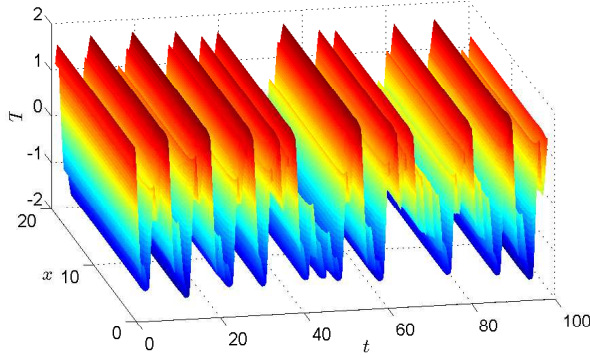
Figure 2.6: The integral surface of (221). The chaotic behavior in the SST is observable in the figure.

2.2.2 Unpredictability Due to the Current Velocity

This subsection is devoted to the investigation of SST when the current velocity behaves chaotically. Here, we will make use of the unpredictable function $\phi(t)$ defined by (213) to apply perturbations to the zonal and vertical components of current velocity in Equation (23).

We begin with considering the equation

$$\frac{\partial T}{\partial t} + [u + \psi(\phi(t))]\frac{\partial T}{\partial x} + v\frac{\partial T}{\partial y} + w\frac{\partial T}{\partial z} = f(t, x, y, z, T), \qquad (222)$$

where, in a similar way to (218), u, v, w, and f are in the form of (28), and $\psi : [-3/4, 3/4] \to \mathbb{R}$ is a continuous function.

One can confirm that Theorem 1 can be used to verify the existence of Poincaré chaos in the dynamics of (222) since it can be reduced by means of the method of characteristics to a system of the form (211) with

$$H(t) = \begin{bmatrix} \psi(\phi(t)) \\ 0 \\ 0 \\ 0 \end{bmatrix},$$

which is an unpredictable function provided that ψ satisfies the condition (219).

In order to demonstrate the chaotic dynamics of (222), we take $u = -0.003\,x + 0.2\sin(\frac{x}{3}) + 0.4$, $v = -0.001\,y$, $w = -0.002\,z - \frac{0.2}{3}\cos(\frac{x}{3})\,z$, $\psi(s) = 3s$, $f =$
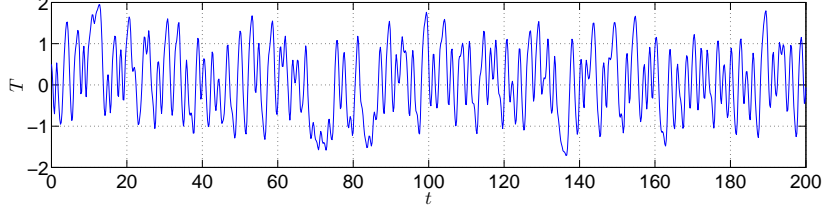
31

Figure 2.7: The solution of (222) with $T(0, 0, 0, 0) = 0.5$. The chaotic behavior of the solution is apparent in the figure.

$-1.5\,T - 3\sin(3x) + 0.2$, and consider the equation

$$\frac{\partial T}{\partial t} + [u + \psi(\vartheta(t))]\frac{\partial T}{\partial x} + v\frac{\partial T}{\partial y} + w\frac{\partial T}{\partial z} = f(t, x, y, z, T), \qquad (223)$$

where $\vartheta(t)$ is the function shown in Figure 2.4.

The time series of the solution of (223) with $T(0, 0, 0, 0) = 0.5$ is depicted in Figure 2.7. One can observe in the figure that the time series is chaotic, and this confirms the result of Theorem 1 such that Equation (222) possesses an unpredictable solution. More precisely, the perturbation of the zonal velocity component in Equation (23) by the unpredictable function $\psi(\phi(t))$ affects the dynamics in such a way that the perturbed equation (222) is Poincaré chaotic.

Next, we will examine the case when the vertical velocity component in Equation (23) is perturbed by the unpredictable function $\phi(t)$. For this aim we set up the equation

$$\frac{\partial T}{\partial t} + u\frac{\partial T}{\partial x} + v\frac{\partial T}{\partial y} + [w + \psi(\phi(t))]\frac{\partial T}{\partial z} = f(t, x, y, z, T), \qquad (224)$$

where the function $\psi : [-3/4, 3/4] \to \mathbb{R}$ is continuous. If we take $u = -0.001\,x + 0.2\sin(\frac{x}{3}) + 0.4$, $v = -0.001\,y$, $w = -0.03z - \frac{0.2}{3}\cos(\frac{x}{3})z$, $\psi(s) = 3s$, and $f = -1.7\,T + 0.5\,z + 1.6$, then Equation (224) admits an unpredictable solution in accordance with Theorem 1.

We represent in Figure 2.8 the solution of the equation

$$\frac{\partial T}{\partial t} + u\frac{\partial T}{\partial x} + v\frac{\partial T}{\partial y} + [w + \psi(\vartheta(t))]\frac{\partial T}{\partial z} = f(t, x, y, z, T), \qquad (225)$$

corresponding to the initial data $T(0, 0, 0, 0) = 0.5$. Here, we use the same u, v, w, ψ, and f as in (224), and $\vartheta(t)$ is again the function whose time series is depicted in
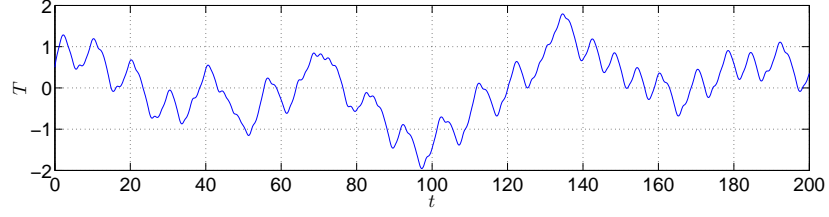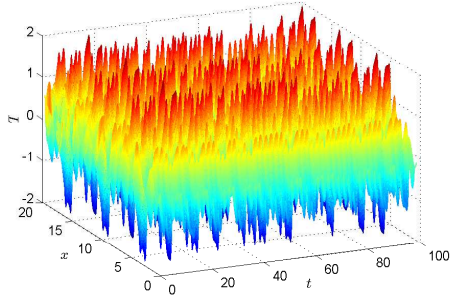
Figure 2.8: Chaotic behavior of SST due to the perturbation of the vertical component of current velocity. The figure shows the solution of (225) with $T(0,0,0,0) = 0.5$.

Figure 2.4. The irregular fluctuations seen in the figure uphold the result of Theorem 1.
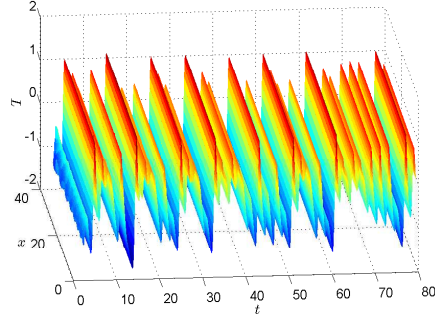
We end up this subsection by illustrating the influence of the chaotic current velocity on the integral surface of SST. Figure 2.9 (a) shows the integral surface of (222) with $u = 1.5 + 0.5\sin x$, $v = 0$, $w = 1 - 0.5\cos x$, $\psi(s) = 2s$, and $f = -1.2\,T - 3\sin(3x)$ at $z = 0$. The initial condition $T(0, x, y, z) = \sin(xz) + 1$ and the boundary conditions $T(t, 0, y, z) = T(t, x, y, 0) = 0.5$ are utilized in the simulation. One can see in Figure 2.9 (a) that the SST has chaotic behavior in keeping with the result of Theorem 1. On the other hand, using the same initial and boundary conditions, we represent in Figure 2.9 (b) the integral surface of (224) with $u = 1$, $v = 0$, $w = 1$, $\psi(s) = 2s$, and $f = -1.2\,T + 3\sin(3z)$ at $z = 1.5$. Figure 2.9 (b) also manifests that the applied perturbation on the vertical component of current velocity make the Equation (224) behave chaotically even if it is initially non-chaotic in the absence of the perturbations.

2.3 Chaotic Dynamics of the Globe Ocean Parameters

Chaotic behavior may transmit from one model to another [27]. This transmission interprets, for instance, why the unpredictability in one stock market or in the weather of one area is affected by another. Chaos in SST may be gained from another endogenous chaotic system like air temperature or wind speed. We can deal with the global ocean as a finite union of subregions. Each of these subregions may be controlled by different models depending on the position and circumstances. An assumption of the existence of chaotic and non-chaotic subregions for SST behavior is very probable.

(a) The integral surface of (222) at $z = 0$ (b) The integral surface of (224) at $z = 1.5$

Figure 2.9: Chaotic behavior of SST due to the current velocity with initial condition $T(0, x, y, z) = \sin(xz) + 1$, and boundary conditions $T(t, 0, y, z) = T(t, x, y, 0) = 0.5$. Both pictures in (a) and (b) reveal that chaotic behavior in the current velocity leads to the presence of chaos in SST.

However, it seems quite unreasonable to imagine a predictable SST for one region whereas its neighbor region is characterized by an unpredictable SST. The mutual effect in SST between neighbor regions can be seen by coupling their controlling models.

2.3.1 Extension of Chaos in Coupled Advection Equations

In this part of the research we deal with the extension of chaos in coupled advection equations. For that purpose, we consider a Poincaré chaotic advection equation of the form (218) as the drive, and we take into account the equation

$$\frac{\partial \tilde{T}}{\partial t} + \tilde{u}\frac{\partial \tilde{T}}{\partial x} + \tilde{v}\frac{\partial \tilde{T}}{\partial y} + \tilde{w}\frac{\partial \tilde{T}}{\partial z} = \tilde{f}(t, x, y, z, \tilde{T}) + g(T) \qquad (226)$$

as the response, in which g is a continuous function and T is a solution of the drive equation (218). We assume that the response does not possess chaos in the absence of the perturbation, i.e., we suppose that the advection equation

$$\frac{\partial \tilde{T}}{\partial t} + \tilde{u}\frac{\partial \tilde{T}}{\partial x} + \tilde{v}\frac{\partial \tilde{T}}{\partial y} + \tilde{w}\frac{\partial \tilde{T}}{\partial z} = \tilde{f}(t, x, y, z, \tilde{T}) \qquad (227)$$

is non-chaotic.

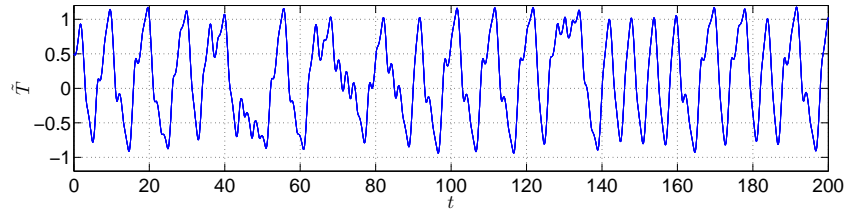34

Figure 2.10: Chaos extension between neighbor regions

Figure 2.11: The solution of the response equation (226) with initial condition $\tilde{T}(0, 0, 0, 0) = 0.5$. The figure manifests the extension of chaos in the coupled system (218)-(226).

Figure 2.10 shows the extension of unpredictability between neighbor regions schematically. We assume that the dynamics of the chaotic region is governed by the drive equation (218), which has an unpredictable solution, and the dynamics of the non-chaotic region is governed by Equation (227). The coupling between these two equations leads to the transmission of unpredictability such that the response system (226) possesses chaos.

To demonstrate the extension of chaos numerically, let us consider the response equation (226) with $u = 1.2$, $v = 0$, $w = 0.3$, $f = -1.5\tilde{T} + 0.2$, and $g(T) = T$. Using the solution T of Equation (221) satisfying $T(0, 0, 0, 0) = 0.5$ as the perturbation in Equation (226), we depict in Figure 2.11 the solution $\tilde{T}$ of (226) corresponding to the initial data $\tilde{T}(0, 0, 0, 0) = 0.5$. Figure 2.11 reveals the extension of chaos in the coupled system (218)-(226).

2.3.2 Coupling of the Advection Equation with Vallis Model

The Lorenz-like form of the Vallis model is given by [51]

$$\frac{du}{dt} = B\, T_d - C\, u,$$
$$\frac{dT_d}{dt} = u\, T_s - T_d, \qquad (228)$$
$$\frac{dT_s}{dt} = -u\, T_d - T_s + 1,$$

where u represents the zonal velocity, $T_d = (T_e - T_w)/2$, $T_s = (T_e + T_w)/2$, T_e and T_w are the SST in the eastern and western ocean respectively, and B and C are constants. System (228) is comparable to the Lorenz system and it was shown by Vallis [50, 51] that (228) with the parameters $B = 102$ and $C = 3$ is chaotic. In paper [99] the authors studied the system (228) with the same parameters and by using the computer-assisted proofs that follow the standard Mischaikow-Mrozek-Zgliczynski approach they located, in the dynamics of the system, topological horseshoes in iterates of Poincaré return maps such that chaos was detected. They considered the chaos with the standard Li-Yorke conditions and said that the dynamics is complicated at least as the dynamics of the full shift on the space of two symbols. The existence of chaos in the dynamics of the Vallis system was also investigated in other studies such as [100, 101].

Next, we take into account the equations

$$\frac{\partial T_1}{\partial t} + 1.2\frac{\partial T_1}{\partial x} + 0.3\frac{\partial T_1}{\partial z} = -1.2\, T_1 - 1 + 2\sin x, \qquad (229)$$

$$\frac{\partial T_2}{\partial t} + 1.2\frac{\partial T_2}{\partial x} + 0.3\frac{\partial T_2}{\partial z} = -2\, T_2 + 4\sin x, \qquad (230)$$

$$\frac{\partial T_3}{\partial t} + 0.6\frac{\partial T_3}{\partial x} + 0.5\frac{\partial T_3}{\partial z} = -2\, T_3 - 1 + 3\sin x, \qquad (231)$$

and

$$\frac{\partial T_4}{\partial t} + 1.2\frac{\partial T_4}{\partial x} + 0.3\frac{\partial T_4}{\partial z} = -1.5\, T_4. \qquad (232)$$

One can verify that the equations (229), (230), (231), and (232) are all non-chaotic such that they admit asymptotically stable regular solutions. By applying perturbations to these equations, we set up the following ones:

$$\frac{\partial T_1}{\partial t} + 1.2\frac{\partial T_1}{\partial x} + 0.3\frac{\partial T_1}{\partial z} = -1.2\, T_1 - 1 + 2\sin x + 4.6\, T_s, \qquad (233)$$
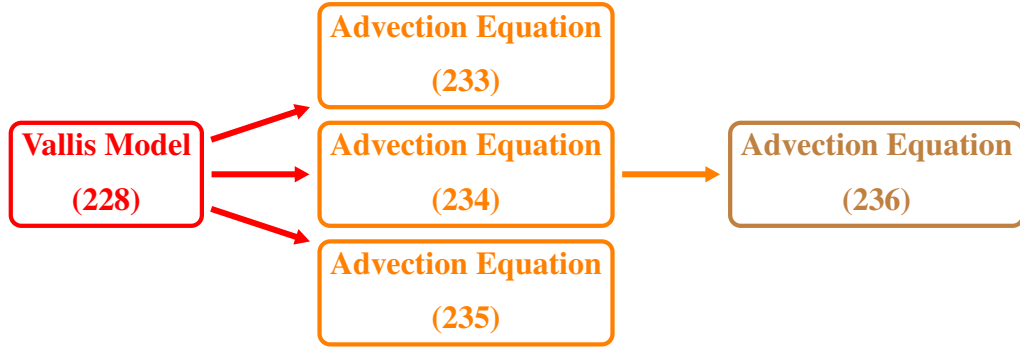
36

Figure 2.12: Chaos extension through coupled systems

$$\frac{\partial T_2}{\partial t} + (1.2 + 0.8\,u)\frac{\partial T_2}{\partial x} + 0.3\frac{\partial T_2}{\partial z} = -2\,T_2 + 4\sin x, \tag{234}$$

$$\frac{\partial T_3}{\partial t} + (0.6 + u)\frac{\partial T_3}{\partial x} + 0.5\frac{\partial T_3}{\partial z} = -2\,T_3 - 1 + 3\sin x + 4\,T_s, \tag{235}$$

$$\frac{\partial T_4}{\partial t} + 1.2\frac{\partial T_4}{\partial x} + 0.3\frac{\partial T_4}{\partial z} = -1.5\,T_4 + 2.7\,T_2, \tag{236}$$

where (u, T_d, T_s) is the solution of the chaotic Vallis model (228) with $B = 102$, $C = 3$ and the initial conditions $u(0) = 2$, $T_d(0) = 0.2$, and $T_s(0) = 0.4$.

In Equation (233) the forcing term is perturbed by the SST average, T_s, whereas in Equation (234) the zonal velocity of Vallis model, u, is used as perturbation. On the other hand, in Equation (235) both the forcing term and the zonal velocity components are perturbed with the solution of (228). Moreover, the solution T_2 of (234) is used as a perturbation in the forcing term of Equation (236). The appearance of the zonal velocity u of the model (228) in the coefficients of Eqs. 234 and 235 looks reasonable if one remembers that the parts of the ocean surface under consideration are adjoining to each other, and consequently, the zonal velocity u perturbs its counterpart in the neighbor region from 1.2 to $1.2 + 0.8u$ in Eq. 234 and from 0.6 to $0.6 + u$ in Eq. 235. Furthermore, the perturbations with T_s in Eqs. 233 and 235 can be attributed to the heat transfer between the neighbor regions because of the structure of the original equation (23). A schematic representation of these coupled systems is given in Figure 2.12.
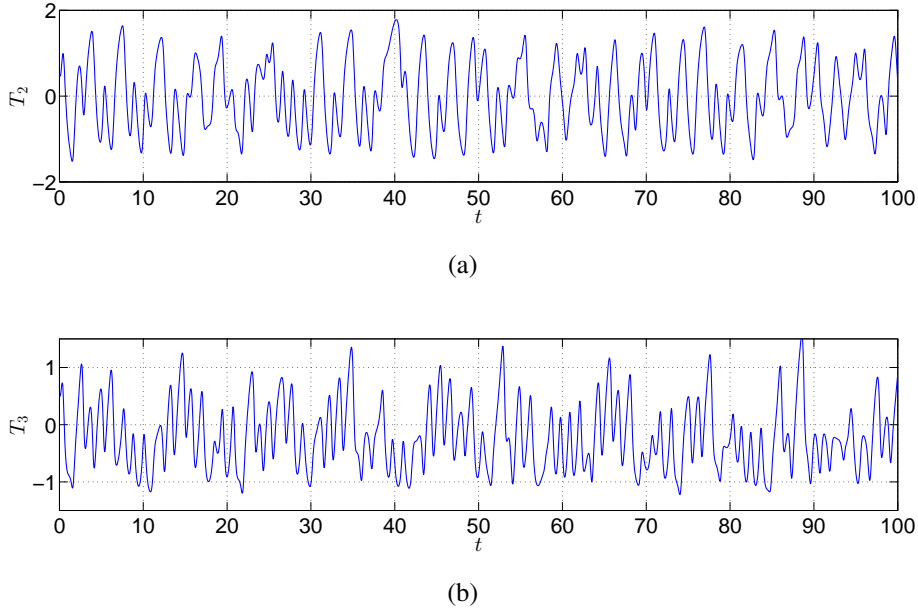
Figure 2.13: The extension of the chaotic behavior by Equations (234) and (235). (a) The time series of the solution of Equation (234), (b) The time series of the solution of Equation (235). The initial data $T_2(0, 0, 0, 0) = 0.5$ and $T_3(0, 0, 0, 0) = 0.5$ are used.

Figure 2.13 (a) and (b) respectively show the solutions T_2, T_3 of Equations (234) and (235), respectively. The initial data $T_2(0, 0, 0, 0) = 0.5$ and $T_3(0, 0, 0, 0) = 0.5$ are used in the simulation. Figure 2.13 reveals that the chaos of the model (228) is extended by Equations (234) and (235).

On the other hand, we depict in Figure 2.14 (a) and (b) the 3 dimensional integral surfaces corresponding to Equations (233) and (236), respectively. Here, we make use of the conditions $T_1(0, x, z) = T_1(t, 0, z) = T_1(t, x, 0) = 0.5$ and $T_4(0, x, z) = T_4(t, 0, z) = T_4(t, x, 0) = 0.5$. The figure confirms one more time that the chaos of system (228) is extended.

2.3.3 Coupling of Vallis Models

Our purpose in this subsection is to demonstrate numerically our suggestion that chaos can be extended between the regions of some global climate variability. We
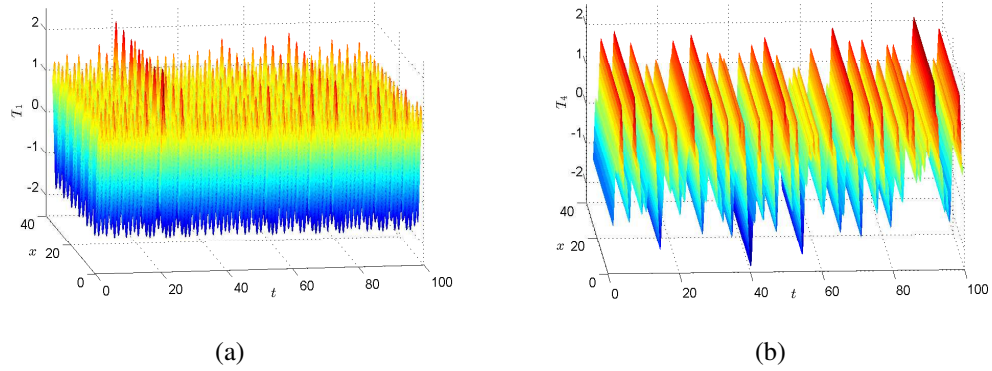
Figure 2.14: Extension of chaos by Equations (233) and (236). (a) The integral surface of Equation (233), (b) The integral surface of Equation (236).
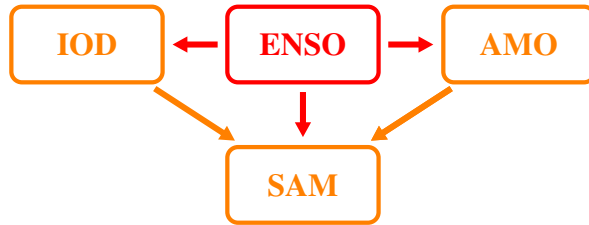

Figure 2.15: Diagram of possible chaos extensions through global climate patterns regions

assume that there are intermediate subregions located between these main regions and chaos can transmit from one region to another in a sequential way.

We also suggest that the IOD can be described by a Vallis model in the form of (228) with parameters appropriate to the Indian Ocean. Evaluation of these parameters is rather difficult. However, for simplicity we can choose these values such that system (228) does not exhibit chaotic behavior. Similar arguments can also be supposed for the AMO and SAM.

A diagram of possible chaos extensions between the regions of IOD, AMO, and SAM are shown in Figure 2.15. In this diagram, the Vallis model representing ENSO is assumed to be the main source of the chaotic behavior, while the Vallis models representing the behaviors of the regions of IOD, AMO, and SAM are all assumed to be initially non-chaotic when interactions do not occur between the regions.

To demonstrate the extension of chaos, let us consider the perturbed Vallis system

$$
\begin{aligned}
\frac{d\tilde{u}}{dt} &= \tilde{B}\,\tilde{T}_d - \tilde{C}\,\tilde{u} + 1.5\,u, \\
\frac{d\tilde{T}_d}{dt} &= \tilde{u}\,\tilde{T}_s - \tilde{T}_d + 0.3\,T_d, \\
\frac{d\tilde{T}_s}{dt} &= -\tilde{u}\,\tilde{T}_d - \tilde{T}_s + 1 + 0.2\,T_s,
\end{aligned}
\tag{237}
$$

where (u, T_d, T_s) is the solution of the chaotic Vallis system (228) with $B = 102$ and $C = 3$ corresponding to the initial conditions $u(0) = 2$, $T_d(0) = 0.2$ and $T_s(0) = 0.4$. We use the parameters $\tilde{B} = 20$ and $\tilde{C} = 7$ in (237) and assume that the unperturbed Vallis model

$$
\begin{aligned}
\frac{d\tilde{u}}{dt} &= \tilde{B}\,\tilde{T}_d - \tilde{C}\,\tilde{u}, \\
\frac{d\tilde{T}_d}{dt} &= \tilde{u}\,\tilde{T}_s - \tilde{T}_d, \\
\frac{d\tilde{T}_s}{dt} &= -\tilde{u}\,\tilde{T}_d - \tilde{T}_s + 1,
\end{aligned}
\tag{238}
$$

represents the SST and zonal velocity variabilities associated with the dynamics of IOD. With these parameter values one can verify that the system (238) has an asymptotically stable equilibrium point at $(1.363, 0.477, 0.350)$, and therefore, it is non-chaotic. Figure 2.16 shows the trajectory of (238) corresponding to the initial conditions $\tilde{u}(0) = 2$, $\tilde{T}_d(0) = 0.2$, $\tilde{T}_s(0) = 0.4$, and it confirms the presence of the asymptotically stable equilibrium point. It is rigorously proven in paper [27] that the Li-Yorke chaos can be transmitted from a chaotic generator to a non-chaotic replicator with asymptotically stable equilibrium, and since the chaos exhibited by (228) satisfies the Li-Yorke conditions, system (237) will inherit the same chaotic behavior as (228). In Fig. 2.17, we represent the time series of $\tilde{u}$, $\tilde{T}_d$, and $\tilde{T}_s$ coordinates of the solution of system (237). One can see in Fig. 2.17 that system (237) possesses chaotic behavior.

2.4 Ocean-Atmosphere Unpredictability Interaction

In this section, we discuss the possibility of the "vertical" extension of unpredictability, i.e. the transmission of chaotic dynamics from ocean to atmosphere and vice versa. To demonstrate this interaction we apply the Lorenz system for the atmosphere and the Vallis model for the ocean. Vallis model is constructed for the domain
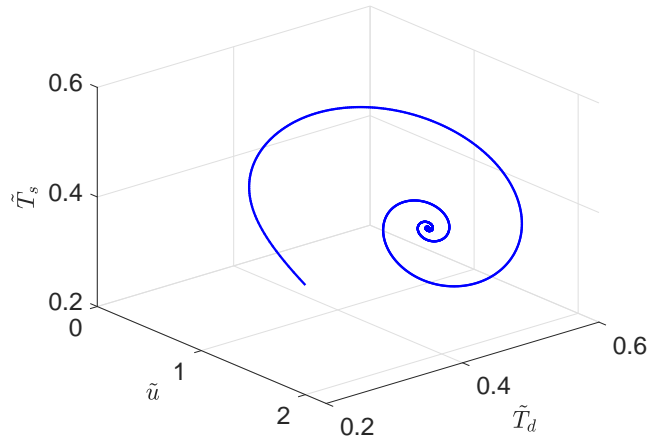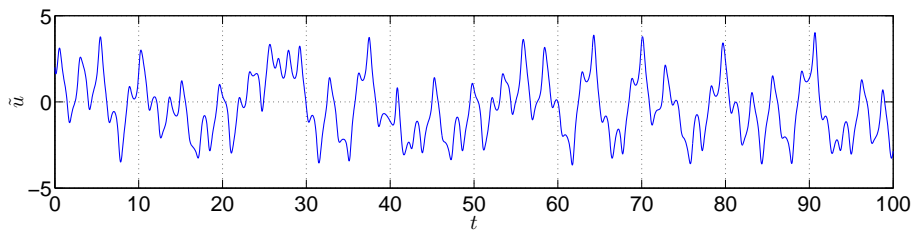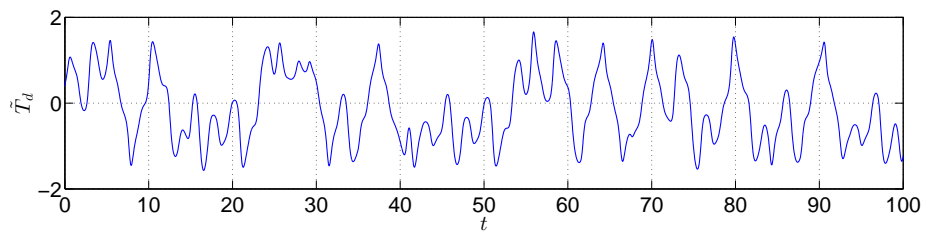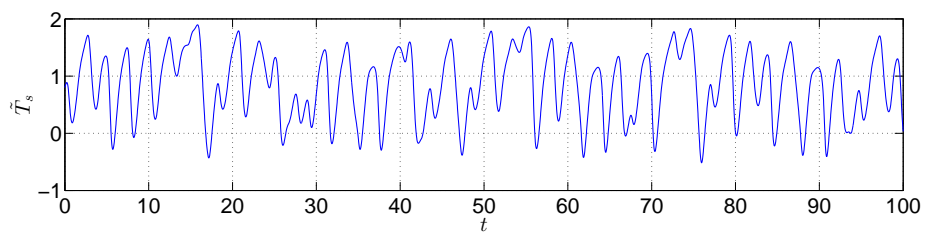
Figure 2.16: The asymptotically stable equilibrium of system (238).

(a)

(b)

(c)

Figure 2.17: The solution of system (237) which reveals chaos extension between a pair of Vallis systems.
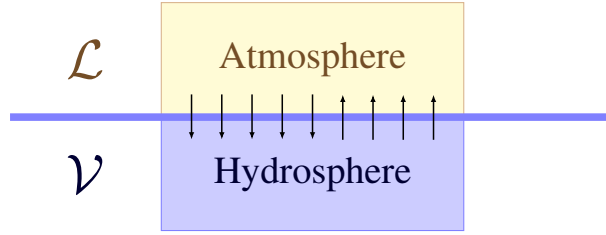
Figure 2.18: Schematic representation of ocean-atmosphere interactions

length of $7500\,\mathrm{km}$, however, depending on the method of construction, the model can be applied for more localized region to be compatible with the Lorenz model. There are two interacted regions shown in Figure 2.18, the atmosphere box $\mathcal{L}$ and the ocean box $\mathcal{V}$, whose dynamics are governed the Lorenz system (21) and the Vallis system (228), respectively.

Heat and momentum exchanges are two important ways of interaction between ocean and atmosphere. The heat exchange is mainly controlled by the air-sea temperature gradient, and, on the other hand, the momentum transfer is determined by the sea-surface stress caused by wind and currents [102]. These characteristics are represented in both Lorenz system (21) and Vallis model (228). Two coordinates in the Lorenz system represent temperature, whereas the third one is related to velocity, and the same could be said for the Vallis system. Therefore, the interaction between ocean and atmosphere can be modeled by coupling the Lorenz and Vallis models.

Let us consider the coupled Lorenz-Vallis systems

$$
\begin{aligned}
\frac{dx}{dt} &= \sigma(y - x) + f_1(u, T_d, T_s), \\
\frac{dy}{dt} &= x(r - z) - y + f_2(u, T_d, T_s), \\
\frac{dz}{dt} &= xy - b\,z + f_3(u, T_d, T_s),
\end{aligned}
\tag{239}
$$

and

$$
\begin{aligned}
\frac{du}{dt} &= B\,T_d - C\,u + g_1(x, y, z), \\
\frac{dT_d}{dt} &= u\,T_s - T_d + g_2(x, y, z), \\
\frac{dT_s}{dt} &= -u\,T_d - T_s + 1 + g_3(x, y, z),
\end{aligned}
\tag{240}
$$

42

where f_i, g_i, $i = 1, 2, 3$, are continuous functions. The coupled model (239)–(240) is in a sufficiently general form of interaction between the $\mathcal{L}$ and $\mathcal{V}$ regions shown in Figure 2.18, where the functions f_i, g_i, $i = 1, 2, 3$ are given in most general form.

To demonstrate the transmission of chaos between the atmosphere and ocean, we consider specific forms of the coupled model (239)–(240). This technique relies on the theoretical investigations of replication of chaos introduced in [27].

In the case of upward transmission of chaos from the ocean to the atmosphere, we consider (239) with specific choices of the perturbation functions f_1, f_2 and f_3 to set up the following system,

$$
\begin{aligned}
\frac{dx}{dt} &= \sigma(y - x) + 3\sin u, \\
\frac{dy}{dt} &= x(r - z) - y + 6\,T_d, \\
\frac{dz}{dt} &= xy - b\,z + 0.5\,T_s^2,
\end{aligned}
\tag{241}
$$

where (u, T_d, T_s) is the solution of the chaotic Vallis system (228) with $B = 102$, $C = 3$ and the initial data $u(0) = 2$, $T_d(0) = 0.2$, $T_s(0) = 0.4$. We use the parameter values $\sigma = 10$, $r = 0.35$ and $b = 8/3$ in (241) such that the corresponding unperturbed Lorenz system (21) does not possess chaos [103].

Figure 2.19 shows the time series of the x, y, and z components of the solution of system (241). The initial data $x(0) = 0$, $y(0) = 0.5$, $z(0) = 0.3$ are used in the figure. The irregular behavior in each component reveals that the chaotic behavior of the atmosphere can be gained from the chaoticity of the hydrosphere characteristics.

For the downward chaos transmission from the atmosphere to the ocean, we consider the perturbed Vallis system

$$
\begin{aligned}
\frac{du}{dt} &= B\,T_d - C\,u + 0.7x, \\
\frac{dT_d}{dt} &= u\,T_s - T_d + 0.3\cos y + 0.4y, \\
\frac{dT_s}{dt} &= -u\,T_d - T_s + 1 + 0.5z,
\end{aligned}
\tag{242}
$$

where (x, y, z) is the solution of the Lorenz system (21) with the parameters $\sigma = 10$, $r = 28$ and $b = 8/3$ and the initial data $x(0) = 0$, $y(0) = 1$, $z(0) = 0$. System (21) possesses a chaotic attractor with these choices of the parameter values [13, 103].

43
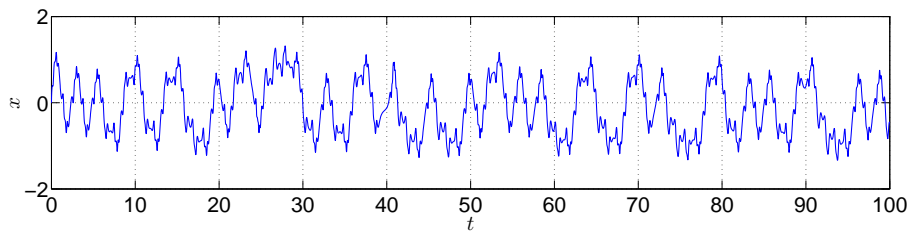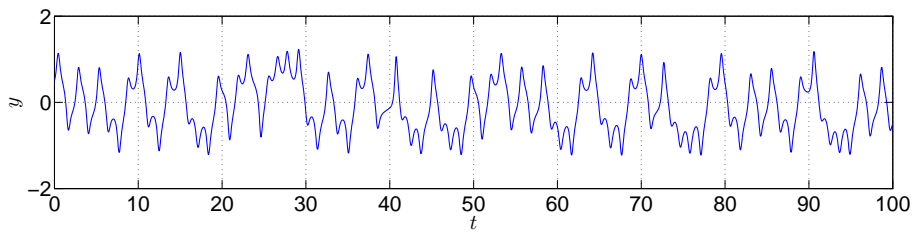
Figure 2.19: The chaotic solution of the perturbed Lorenz system (241).
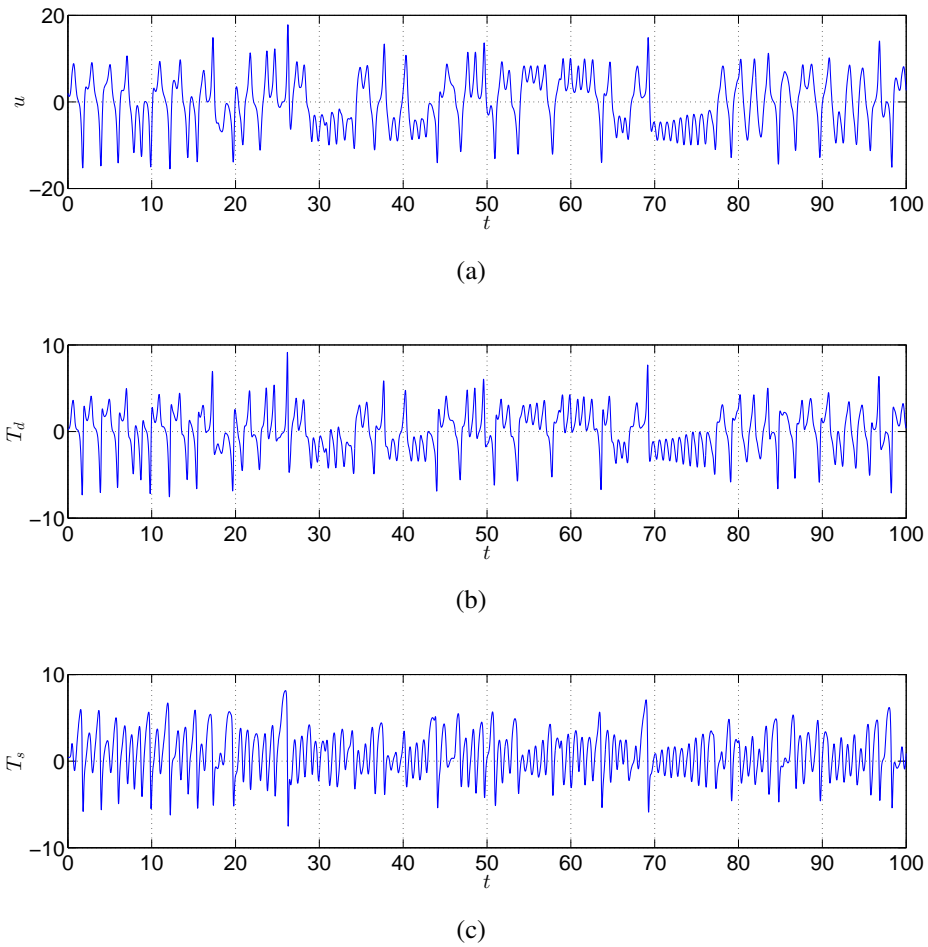
Figure 2.20: Chaotic behavior of system (242).

Let us take $B = 20$ and $C = 7$ in system (242). One can verify in this case that the corresponding unperturbed system (228) is non-chaotic such that it possesses an asymptotically stable equi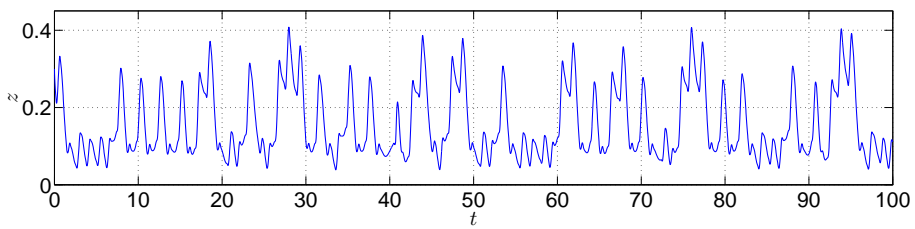librium. Figure 2.20 depicts the solution of (242) with $u(0) = 2$, $T_d(0) = 0.2$, and $T_s(0) = 0.4$. It is seen in Figure 2.20 that the chaotic behavior of the Lorenz system (21) is transmitted to (242). In other words, system (242) admits chaos even if it is initially non-chaotic in the absence of the perturbation.

2.5 Conclusion

In this chapter we discuss the possible unpredictable behavior of climate variables on a global scale. Some ENSO-like climate variabilities have a significant influ-

ence on global weather and climate. ENSO variability is suggested to be chaotic by many studies. The well-known Vallis ENSO chaotic model is one among several ENSO models that exhibit irregular behavior. The presence of chaos in ENSO can be indicated by the behavior of SST as well as ocean current velocity. We describe the dynamics of SST by the advection equation. The forcing term, based on ocean-atmosphere interaction, and the current velocity in this equation can be a source of unpredictability in SST. We prove the presence of chaos in SST dynamics by utilizing the concept of unpredictable function. The relationship and interaction between the climate variabilities, like the ones between ENSO and IOD, have attracted attention in recent literature. Constructing and understanding the dynamic models driving these phenomena are the main steps to investigate the mutual influences between these global events. The SST anomalies are closely linked to some climate variabilities teleconnections in different parts of the global ocean. We suggest that the hydrosphere characteristics can behave chaotically through the possibility of transmission of chaos between ocean neighbor subregions. We verified this transmission by different "toy" couples of advection equations and Vallis models. The simulations of these couples show that unpredictability can be transmitted from a local region controlled by a chaotic model into its neighbor which is described by a non-chaotic model.

The mechanism of unpredictability extension can be interpreted in terms of physical operations. The simplicity of the models under consideration, namely the Vallis model and the advection equation, allows to make the physics much clearer. The onset of ENSO is accompanied with zonal SST gradient over the equatorial Pacific Ocean. The same situation applies to IOD in Indian Ocean and other similar climate patterns. This distribution of SST leads to heat transport by convection in the mixed layer and ocean circulation through its effect on surface wind and ocean atmospheric circulation. These physical processes, which include heat, mass and momentum transfer, can be accompanied with "*chaos transfer*". We believe that this thought still needs a consistent theoretical framework to understand all features of such operation, principally the intrinsicness of chaos for these physical quantities. Nevertheless, the presented mechanism of unpredictability extension could be seen as a step towards this goal. Further steps can be performed by including different models for more climate components.

We proposed to apply the same technique for the "vertical" unpredictability exchange between atmosphere and hydrosphere. In this case, the Lorenz system and the Vallis model are assigned for the atmosphere and ocean, respectively. Physically, this exchange may be done in the midst of interaction between ocean and atmosphere associated with, for example, heat exchange. By this procedure, the global unpredictability of oceanic oscillation can be viewed as accompaniment to weather unpredictability.

Our approach provides a basic frame for mathematical interpretation to the irregular behavior of some global climate characteristics. It gives a way to link the local unpredictability in a component of climate system to more global scope. Further investigation can done by including different models for more climate components. Another important and interesting problem is *controlling weather*. Even though the weather is too complicated to modify, a vital step can be taken toward this goal by modify the ENSO oscillation through control of chaos in its models and study the "extension of the control" between ENSO-like models and weather models. Chaos control in Lorenz system is still not effectively developed in the literature, where the most proposed methods are mainly depend on forcing the system into a single stable periodic behavior [25, 104], and this is not adequate for real life applications. It is known that the chaos control can be achieved by using small perturbation to some parameters or variables of the system. This idea may be practically applied by making a small local artificial effect in atmosphere or hydrosphere. If we consider the positive tenor of the Lorenz's famous question, "Does the flap of a butterfly's wing in Brazil set off a tornado in Texas?", we can say that the small artificial climate change may prevent the occurrence or at least decrease the intensity of some extreme weather events such as cyclones, hurricanes, droughts, and floods.

CHAPTER 3

FRACTALS: DYNAMICS IN THE GEOMETRY

3.1 Introduction

French mathematicians Pierre Fatou and Gaston Julia in 917-1918 invented a special iteration in the complex plane [44, 49] such that new geometrical objects with unusual properties can be built. The iteration is called Fatou-Julia Iteration (FJI) [22] or sometimes "Escape Time Algorithm" [24]. One of the famous fractals constructed by the iteration is the Julia set. Besides the iteration of rational maps, there are various ways to construct fractal shapes. The well known self-similar fractals like Sierpinski gasket, Sierpinski carpet, and Koch curve are constructed by means of a simple recursive process which consists in iteratively removing shrinking symmetrical parts from an initial shape. These types of geometrical fractals can also be produced by an Iterated Function System (IFS) [105, 106], which is defined as collections of affine transformations.

There are two sides of the fractal research related to the present study. The first one is FJI and the second one is the proposal by Mandelbrot to consider dimension as a criterion for fractals. In our approach, both factors are crucial as we apply the FJI for the construction of the sets and the dimension factor to confirm that the built sets are fractals. In previous studies the iteration and the dimension factors were somehow separated, since self-similarity provided by the iteration has been self-sufficient to recognize fractals, but in our research the similarity is not true in general. We have to emphasize that there is a third player on the scene, the modern state of computers' power. Their roles are important for the realization of our idea exceptionally for continuous dynamics. One can say that the instrument is at least of the same

(a) Achilles and the tortoise dynamics

(b) The state, S_0, of the dynamics

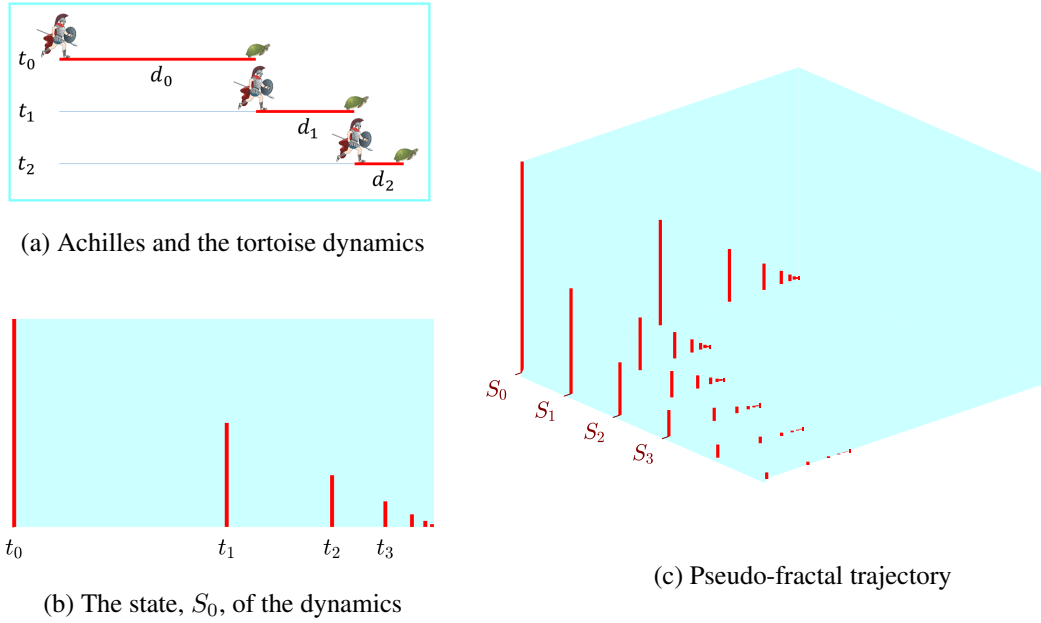

(c) Pseudo-fractal trajectory

Figure 3.1: The dynamics of the Zeno's Paradox

importance for application of our idea to fractals as for realization of Fatou-Julia iteration in Mandelbrot and Julia sets. Nevertheless, we expect that the present study will significantly increase the usage of computers for fractal analysis. Moreover, beside differential equations, our suggestions will effect the software development for fractals investigation and applications [107, 108].

Studying the problem, we have found that fractal-like appearances can be observed in ancient natural philosophy. Let us consider the Achilles and tortoise in the Zeno's Paradox [109, 110], (see Fig. 3.1a).

In the paradox, Achilles is observed at the initial moment $t_0 = 0$ with the distance d_0 from the tortoise. Suppose that Achilles runs at a constant speed, two times faster than the tortoise, then he would reach the previous position of the tortoise at moments t_1, $t_2 = 3t_1/2$, $t_3 = 7t_1/4, ...$ with distances $d_1 = d_0/2$, $d_2 = d_0/4$, $d_3 = d_0/8, ...$ from the tortoise, respectively. Now contemplate Fig. 3.1b, where the heights of the red lines are proportional to the distance of Achilles from the tortoise at the fixed moments, and denote the diagram by S_0. The set S_0 demonstrates the entire dynamics for $t \geq t_0$. Fix $i \geq 0$, and let S_i be the similar diagram which consists of all the lines for the moments which are not smaller than t_i.

Let us consider the collection of the states $\{S_i\}, i \geq 0$. One can assume that there exists a map $\mathcal{B}$ such that the equations

$$S_{i+1} = \mathcal{B}\,S_i,\; i = 0, 1, 2, \ldots,$$

which symbolize a dynamics, are valid. It is easily seen that S_0 is self-similar to each of its parts $S_i,\; i > 0$. Nevertheless, the Hausdorff dimension of the set S_0 is equal to one. For this reason, we call $S_i,\; i \geq 0$, *pseudo-fractals*, due to the similarity. The trajectory $\{S_i\}, i \geq 0$, is also a pseudo-fractal. The sketch of the trajectory is seen in Fig. 3.1c.

The research is an extension of the ancient paradigm, since we will investigate dynamics having all points of a trajectory as well as the trajectory itself fractals.

3.2 Fatou-Julia Iteration

Involvement of the dynamics of iterative maps in fractal construction was a critical step made by Fatou and Julia [44, 49]. They described what we call today FJI. The iteration is defined over a domain $\mathcal{D} \subseteq \mathbb{C}$ by

$$z_{n+1} = F(z_n), \tag{31}$$

where $F : \mathcal{D} \to \mathcal{D}$ is a given function for the construction of the fractal set $\mathcal{F}$. The points $z_0 \in \mathcal{D}$ are included in the set $\mathcal{F}$ depending on the boundedness of the sequence $\{z_n\},\; n = 0, 1, 2, \ldots$, and we say that the set $\mathcal{F}$ is constructed by FJI.

In practice one cannot verify the boundedness for infinitely long iterations. This is why in simulation we fix an integer k and a bounded subset $M \subset \mathbb{C}$, and denote by $\mathcal{F}_k$ the collection of all points $z_0 \in \mathcal{D}$ such that the points z_n where the index n is between 1 and k, $n = 1, 2, \ldots, k$, belong to M. In what follows we call the set $\mathcal{F}_k$ the *kth approximation* of the set $\mathcal{F}$.

The most popular fractals, Julia and Mandelbrot sets, are generated using the iteration of the quadratic map $F(z_n) = z_n^2 + c$, where c is a complex number. The so-called filled-in Julia set, $\mathcal{K}_c$, is constructed by including only the points $z_0 \in \mathbb{C}$ such that the sequence z_n is bounded [111]. Moreover, in the simulation, those points $z_0 \in \mathbb{C}$

where $\{z_n\}$ is divergent are colored in a different way, correspondingly to the rate of divergence. The term Julia set $\mathcal{J}_c$, usually denotes the boundary of the filled Julia set, i.e., $\mathcal{J}_c = \partial \mathcal{K}_c$.

In the case of the Mandelbrot set, $\mathcal{M}$, we include in $\mathcal{M}$ the points $c \in \mathbb{C}$ such that $\{z_n(c)\}$, $z_0(c) = 0$, is bounded. Here again, the points $c \in \mathbb{C}$ corresponding to divergent sequences z_n are plotted in various colors depending on the rate of the divergence.

3.3   How to Map Fractals

To describe our way for mapping of fractals, let us consider a fractal set $\mathcal{F} \subseteq A \subset \mathbb{C}$, constructed by the following FJI,

$$z_{n+1} = F(z_n), \tag{32}$$

where $F : A \to A$ is not necessarily a rational map. We suggest that the original fractal $\mathcal{F}$ can be transformed "recursively" into a new fractal set. For that purpose, we modify the FJI, and consider iterations to be of the form

$$f^{-1}(z_{n+1}) = F\big(f^{-1}(z_n)\big), \tag{33}$$

or explicitly,

$$z_{n+1} = f\Big(F\big(f^{-1}(z_n)\big)\Big), \tag{34}$$

where f is a one-to-one map on A. Next, we examine the convergence of the sequence $\{z_n\}$ for each $z_0 \in f(A)$. Denote by $\mathcal{F}_f$ the set which contains only the points z_0 corresponding to the bounded sequences. Moreover, other points can be plotted in different colors depending on the rate of the divergence of $\{z_n\}$. To distinct the iterations (34) from the Fatou-Julia iterations let us call the first ones *Fractals Mapping Iterations* (FMI). It is clear that FJI is a particular FMI, when the function is the identity map. The mapping of fractals is a difficult problem which depends on infinitely long iteration processes, and has to be accompanied with sufficient conditions to ensure that the image is again fractal.

The next theorem is the main instrument for the detection of fractal mappings. Accordingly, we call it *Fractal Mapping Theorem* (FMT).

Theorem 2. *If f is a bi-Lipschitz function, i.e. there exist numbers $l_1, l_2 > 0$ such that*

$$l_1|u - v| \leq |f(u) - f(v)| \leq l_2|u - v| \tag{35}$$

for all $u, v \in A$, then $\mathcal{F}_f = f(\mathcal{F})$.

Proof. Fix an arbitrary $w \in \mathcal{F}_f$. There exists a bounded sequence $\{w_k\}$ such that $w_0 = w$ and $f^{-1}(w_{k+1}) = F(f^{-1}(w_k))$. Let us denote $z_k = f^{-1}(w_k)$. Our purpose is to show that $\{z_k\}$ is a bounded sequence. Indeed

$$|z_k - z_0| = |f^{-1}(w_k) - f^{-1}(w_0)| \leq \frac{1}{l_1}|w_k - w_0|.$$

Hence, the boundedness of $\{w_k\}$ implies the same property for $\{z_k\}$, and therefore, we have $z_0 = f^{-1}(w) \in \mathcal{F}$.

Now, assume that $w \in f(\mathcal{F})$. There is $z \in \mathcal{F}$ such that $f(z) = w$ and a bounded sequence $\{z_k\}$ such that $z_0 = z$ and $z_{k+1} = F(z_k)$. Consider, $w_0 = w$ and $w_k = f(z_k)$, $k \geq 0$. It is clear that the sequence $\{w_k\}$ satisfies the iteration (33) and moreover

$$|w_k - w_0| = |f(z_k) - f(z_0)| \leq l_2|z_k - z_0|.$$

Consequently, $\{w_k\}$ is bounded, and $w \in \mathcal{F}_f$. $\qquad\square$

The following two simple propositions are required.

Lemma 1. *[112] If f is a bi-Lipschitz function, then*

$$\dim_H f(A) = \dim_H A,$$

where $\dim_H$ denotes the Hausdorff dimension.

Lemma 2. *If $f : A \to \mathbb{C}$ is a homeomorphism, then it maps the boundary of A onto the boundary of $f(A)$.*

It is clear that a bi-Lipschitz function is a homeomorphism.

Shishikura [113] proved that the Hausdorff dimension of the boundary of the Mandelbrot set is 2. Moreover, he showed that the Hausdorff dimension of the Julia set corresponding to $c \in \partial\mathcal{M}$ is also 2.

Routine mapping	Fractal mapping
(i) The preimage description $$\mathcal{F} = \{(x, y) : g(x, y) = 0\}$$	**(a)** The fractal-preimage description $$\mathcal{F} = \{(x, y) : (x_n, y_n),\ \text{where}\ (x_0, y_0) = (x, y)\ \text{and}\ (x_{n+1}, y_{n+1}) = g(x_n, y_n),\ \text{is bounded}\}$$
(ii) The map definition $$f : (u, v) = f(x, y)$$	**(b)** The map definition $$f : (u, v) = f(x, y)$$
(iii) The image description $$\mathcal{F}_f = \{(u, v) : g(f^{-1}(u, v)) = 0\}$$	**(c)** The fractal-image description $$\mathcal{F}_f = \{(u, v) : f^{-1}(u_n, v_n),\ \text{where}\ (u_0, v_0) = (u, v)\ \text{and}\ f^{-1}(u_{n+1}, v_{n+1}) = g(f^{-1}(u_n, v_n)),\ \text{is bounded}\}$$

Table 3.1: The differences between a routine mapping and the fractal mapping

It implies from the above discussions that if f is a bi-Lipschitz function and $\mathcal{F}$ is either a Julia set or the boundary of the Mandelbrot set, then their images $\mathcal{F}_f$ are fractals. In what follows, we will mainly use functions, which are bi-Lipschitzian except possibly in neighborhoods of single points.

To emphasize the novelty concerning the map algorithm (change of coordinates), we suggest the Table 3.1 below, which illustrates the differences between a routine map and the newly constructed fractal mapping.

Let us give comments on the content of Table 3.1 and explain why the mapping of fractals is different than those which can be accepted as routine maps. Consider the two-dimensional case for a set $\mathcal{F}$. In the routine map, the preimage $\mathcal{F}$ is simply given by equation (i) in the table, while for the fractal-preimage description we need the procedure (a) which theoretically consists of an infinite number of steps. The most important difference is manifested in the image description. In the routine mapping, the image can be defined by formula (iii). However, to describe the fractal-image, one should involve the infinite process of the preimage construction (a). The novelty of our approach is exactly in finding how the infinite process can be involved to define
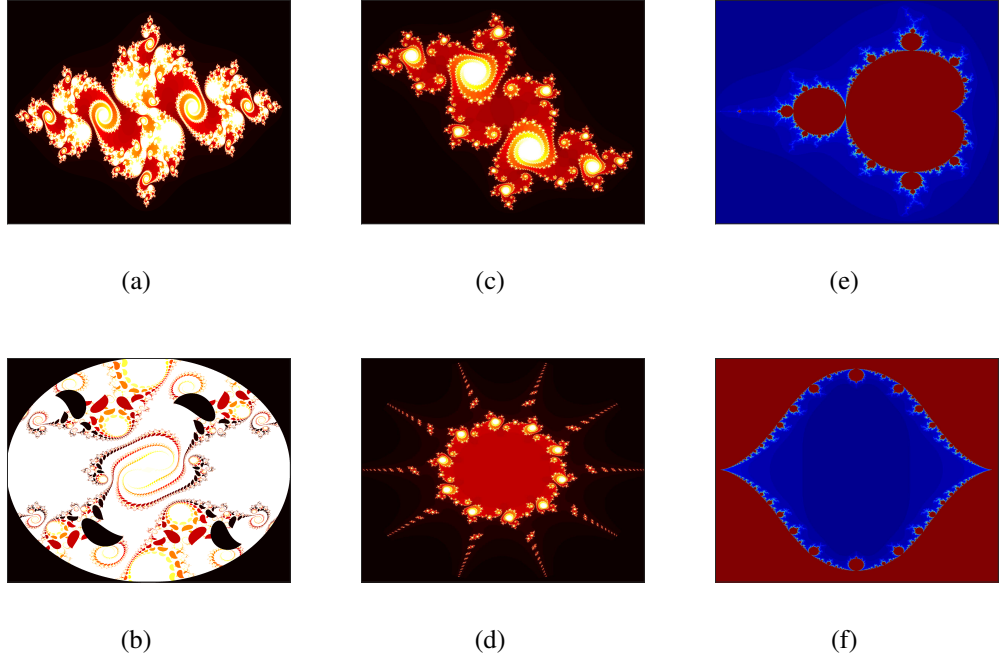
(a)　　　　　　(c)　　　　　　(e)

(b)　　　　　　(d)　　　　　　(f)

Figure 3.2: Julia and Mandelbrot sets with their images

the fractal mapping algorithm (c).

Now, we apply FMI to a Julia set $\mathcal{J}$, and the iteration will be in the form

$$f^{-1}(z_{n+1}) = \left[f^{-1}(z_n)\right]^2 + c, \tag{36}$$

with various functions f and values of c. The resulting fractals $\mathcal{J}_f = f(\mathcal{J})$ are depicted in Fig. 3.2 (b) and (d). They are mapped by $f(z) = \cos^{-1}\left(\frac{1}{z} - 1\right)$, $c = -0.7589 + 0.0735i$, and $f(z) = \left(\sin^{-1} z\right)^{\frac{1}{5}}$, $c = -0.175 - 0.655i$ from the Julia sets in Fig. 3.2 (a) and (c), respectively.

For mapping of the Manderbrot set, we propose the FMI

$$z_{n+1} = z_n^2 + f^{-1}(c). \tag{37}$$

Along the lines of the proof of Theorem 2, one can show that if the map f is bi-Lipschitzian, then the iteration (37) defines the relation $f(\mathcal{M}) = \mathcal{M}_f$, where $\mathcal{M}_f$ is a new fractal. Figure 3.2 (f) shows a fractal mapped by $f(c) = \left(\frac{1}{c} - 1\right)^{\frac{1}{2}}$ from the Mandelbrot set in Fig. 3.2 (e).

55

3.4 Dynamics for Julia sets

3.4.1 Discrete Dynamics

Discrete fractal dynamics means simply iterations of mappings introduced in the last section. Let us consider a discrete dynamics with a bi-Lipschitz iteration function f and a Julia set $\mathcal{J}_0 = \mathcal{J}$ as an initial fractal for the dynamics. The trajectory

$$\mathcal{J}_0, \mathcal{J}_1, \mathcal{J}_2, \mathcal{J}_3, \ldots,$$

is obtained by the FMI

$$z_{n+1} = f^k \Big([f^{-k}(z_n)]^2 + c \Big), \tag{38}$$

such that $\mathcal{J}_{k+1} = f(\mathcal{J}_k)$, $k = 0, 1, 2, 3, \ldots$. The last equation is a fractal propagation algorithm.

The computational procedure of the numerical simulation for the discrete fractal trajectory of Eq. (38) is summarized in Algorithm 1. Figure 3.3, which is obtained by using Algorithm 1, shows the trajectory and its points at $k = 1$ and $k = 5$ for the function $f(z) = z^2 + ac + b$ with $a = 0.6$, $b = 0.02 - 0.02i$ and $c = -0.175 - 0.655i$.

3.4.2 Continuous Dynamics

To demonstrate a continuous dynamics A_t with real parameter t and fractals, we use the differential equation
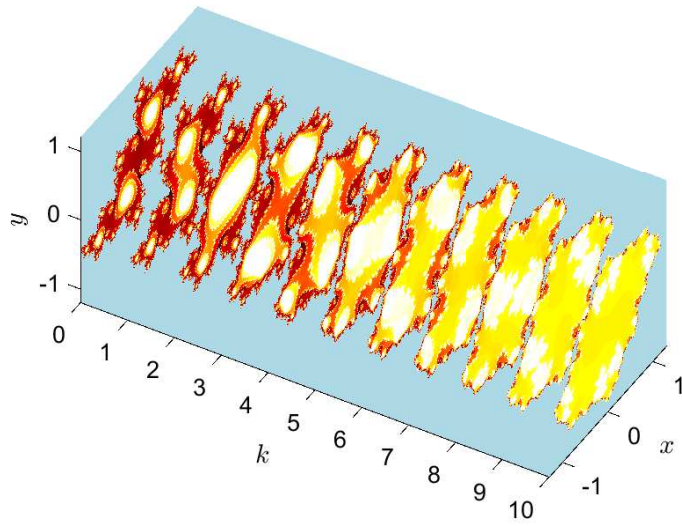
$$\frac{dz}{dt} = g(z), \tag{39}$$

such that $A_t z = \phi(t, z)$, where $\phi(t, z)$ denotes the solution of (39) with $\phi(0, z) = z$. Thus, we will construct dynamics of sets $A_t \mathcal{F}$, where a fractal $\mathcal{F}$ is the initial value. To be in the course of the previous sections, we define a map $f(z) = A_t z$ and the equation
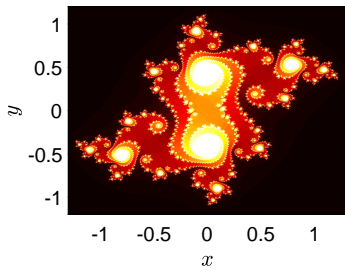
$$A_{-t}(z_{n+1}) = [A_{-t}(z_n)]^2 + c.$$

Thus the FMI (34) in this case will be in the form

$$z_{n+1} = A_t \Big([A_{-t}(z_n)]^2 + c \Big). \tag{310}$$
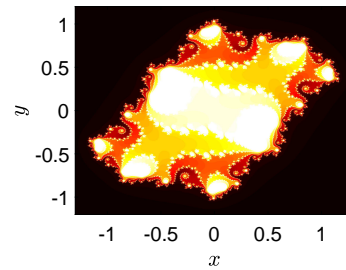
56

(a) Discrete fractal trajectory

(b) $k = 1$

(c) $k = 5$

Figure 3.3: The discrete trajectory

57

Algorithm 1: Discrete dynamics simulation

---

1 Define the map $f(t)$ and its inverse $f^{-1}(t)$

2 Specify the initial Julia set $\mathcal{J}_0$ by setting the parameter c

3 Set the upper bound b

4 Set the number of maximum iterations j_m

5 Create a mesh with $N_p = N \times M$ elements on the domain of $\mathcal{J}_0$

6 Set the number of the map iterations K

7 for $k = 1$ *to* K **do**

8   Initiate the image matrix $Z = \text{zeros}(M, N)$

9   **for** $n = 1$ *to* N_p **do**

10   Pick a point (x, y) from the domain

11   Let $z = x + iy$

12   Set $j = 0$

13   **while** $(j < j_m)$ *and* $(x^2 + y^2 < b^2)$ **do**

14   Let $j = j + 1$

15   Find the image $z = f^k\left(\left(f^{-k}(z)\right)^2 + c\right)$

16   Compute $x = \text{Re}(z)$ and $y = \text{Im}(z)$

17   **end**

18   Assign the image matrix elements, $Z(n) = j$

19   **end**

20   Display the image Z on the x, y, k coordinates

21 end

In what follows, we assume that the map A_t is bi-Lipschitzian. This is true, for instance, if the function g in (39) is Lipschitzian. Then the set $A_t\mathcal{F}$ for each fixed t is a fractal determined by the FMI, and we can say about continuous fractal dynamics. Algorithm 2, which is provided in the Appendix, gives the general outline of the computational steps of the numerical simulation for trajectories generated by the FMI (310). The Algorithm is used to produce the trajectories shown in Figs. 3.4, 3.5, and 3.6.

As an example we consider the differential equation $dz/dt = -z$, $0 \le t \le 1$, with the flow $A_t z = ze^{-t}$. It represents a contraction mapping when it is applied to the iteration (310), whereas the unstable dynamical system $A_t z = ze^t$ corresponding to the differential equation $dz/dt = z$ represents an expansion mapping.

Figure 3.4 (a) and (b) contain fractal trajectories of the dynamics with the initial Julia set $\mathcal{J}$, corresponding to $c = -0.175 - 0.655i$. The initial fractal and the point of the expansion at $t = 1$ are seen in parts (c) and (d) of the figure, respectively.

Now, we will focus on the autonomous system of differential equations

$$\frac{dx}{dt} = -y + x(4 - x^2 - y^2),$$
$$\frac{dy}{dt} = x + y(4 - x^2 - y^2). \tag{311}$$

The solution of the last system in polar coordinates with initial conditions $\rho(0) = \rho_0$ and $\varphi(0) = \varphi_0$ is given by

$$\rho(t) = 2e^{4t}\left(\frac{4}{\rho_0^2} + e^{8t} - 1\right)^{-\frac{1}{2}},$$
$$\varphi(t) = t + \varphi_0.$$

Thus, the map can be constructed by

$$A_t z = x(t) + iy(t), \tag{312}$$

where

$$x(t) = \rho(t)\cos(\varphi(t)),$$
$$y(t) = \rho(t)\sin(\varphi(t)),$$
$$z = \rho_0\cos(\varphi_0) + i\rho_0\sin(\varphi_0).$$

**Algorithm 2:** Continuous dynamics simulation

---

1 Find the solution $\phi(t, z)$ of the used differential equation

2 Define the map as $f(z) = A_t z$, where $A_t z = \phi(t, z)$

3 Define the inverse of the map as $f^{-1}(z) = A_{-t} z$

4 Specify the initial Julia set $\mathcal{J}_0$ by setting the parameter c

5 Set the upper bound b

6 Set the number of maximum iterations j_m

7 Create a mesh with $N_p = N \times M$ elements on the domain of $\mathcal{J}_0$

8 Set the temporal domain $t_0 \leq t \leq T$, with a step size Δt

9 Compute the number of image iteration $N_t = T/\Delta t + 1$

10 Set $t = t_0$

11 **for** $k = 1$ *to* N_t **do**

12   Initiate the image matrix $Z = \text{zeros}(M, N)$

13   **for** $n = 1$ *to* N_p **do**

14   Pick a point (x, y) from the domain

15   Let $z = x + iy$

16   Set $j = 0$

17   **while** *($j < j_m$) and ($x^2 + y^2 < b^2$)* **do**

18   Let $j = j + 1$

19   Find the image $z = A_t\left(\left(A_{-k}(z)\right)^2 + c\right)$

20   Compute $x = \text{Re}(z)$ and $y = \text{Im}(z)$

21   **end**

22   Assign the image matrix elements, $Z(n) = j$

23   **end**

24   Display the image Z on the x, y, t coordinates

25   Let $t = t + \Delta t$
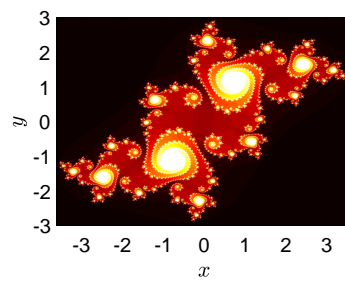
26 **end**
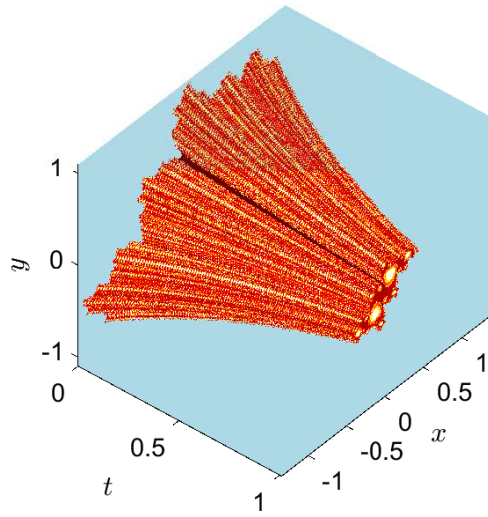
(a) $\mathcal{J}e^{-t}$
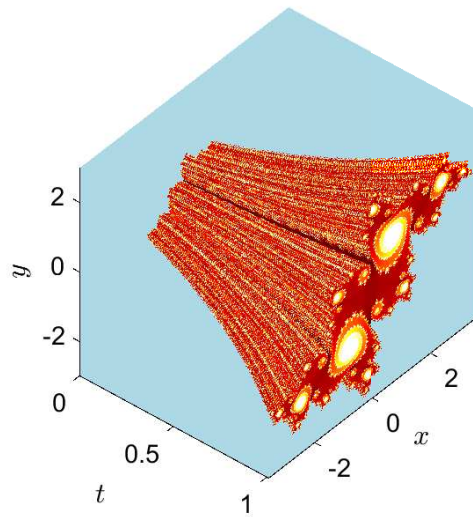
(b) $\mathcal{J}e^{t}$
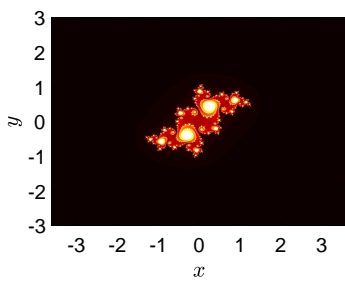
(c) $t = 0$

(d) $t = 1$

Figure 3.4: Fractals of the continuous dynamics

61

In Fig. 3.5 (a), the fractal trajectory of system (311) is seen with the Julia set as the initial fractal. Parts (b)-(g) of the same figure represent various points of the trajectory.

Next, let us consider the non-autonomous differential equation

$$\frac{dz}{dt} = az + (\cos t + i \sin t), \tag{313}$$

and the map

$$A_t z = (z + \frac{a+i}{1+a^2})e^{at} - \frac{a+i}{1+a^2}(\cos t + i \sin t), \tag{314}$$

which is determined by the solutions of Eq. 313.

The map is not of a dynamical system since there is no group property for non-autonomous equations, in general. This is why, Eq. 310 cannot be used for fractal mapping along the solutions of the differential equation (313). However, for the moments of time $2\pi n$, $n = 1, 2, \ldots$, which are multiples of the period, the group property is valid, and therefore iterations by Eq. 310 determine a fractal dynamics at the discrete moments. In the future, finding conditions to construct fractals by non-autonomous systems might be an interesting theoretical and application problem. We have applied the map with $a = 0.01$ and the Julia set corresponding to $c = -0.175 - 0.655i$ as the initial fractal. The results of the simulation are seen in Fig. 3.6. Since the moment $t = \frac{\pi}{2}$ is not a multiple of the period, the section in part (b) of the figure does not seem to be a fractal, but in part (c), the section is a Julia set.

3.5 Dynamics Motivated by Sierpinski Fractals

Fatou-Julia iteration is an effective instrument to construct fractals. Famous Julia and Mandelbrot sets are strong confirmations of this. In this section, we use the paradigm of FJI to construct and map Sierpinski fractals. The processes of the construction of the Sierpinski gasket starting by an initial solid triangle, then dividing it into four identical triangles and removing the central one. In the next iterations, the same procedure is repeated to each of the remaining triangles from the preceding iteration. In an analogous way to the gasket, the construction of the Sierpinski carpet starting by an initial solid square, then dividing it into nine squares and removing the central
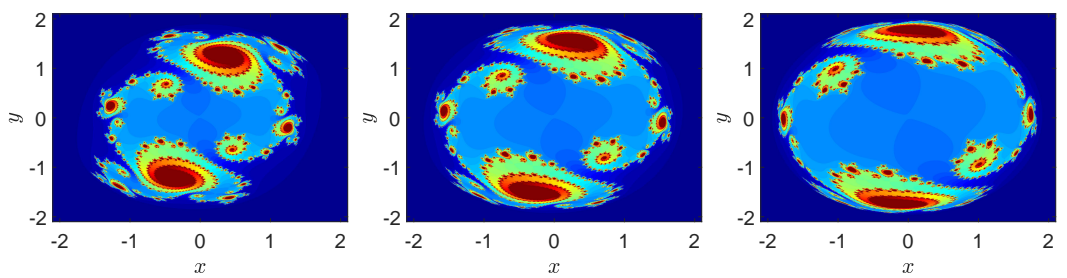
62
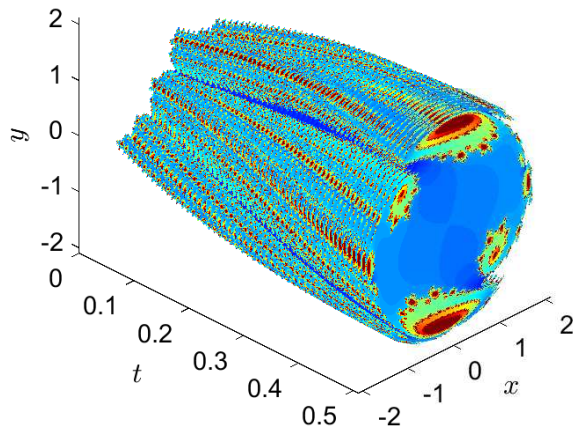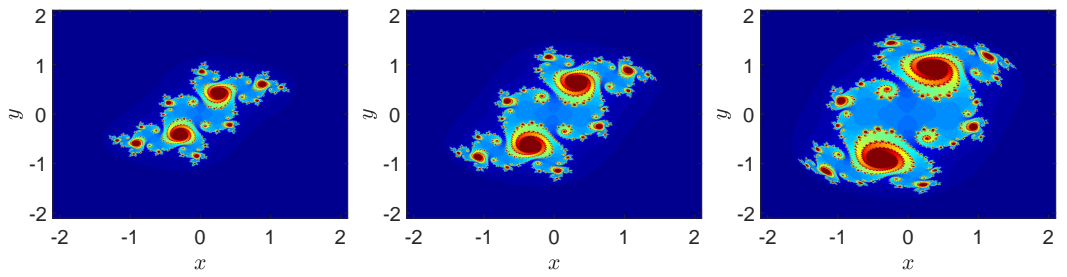
(a) $A_t \mathcal{J}$

(b) $t = 0$

(c) $t = 0.1$

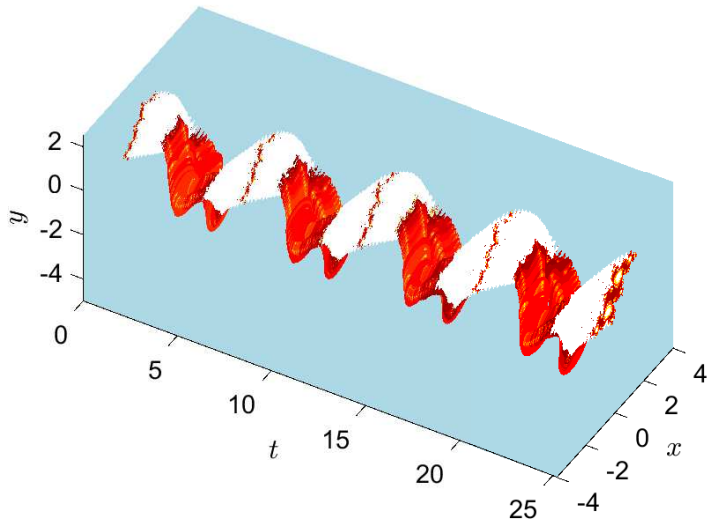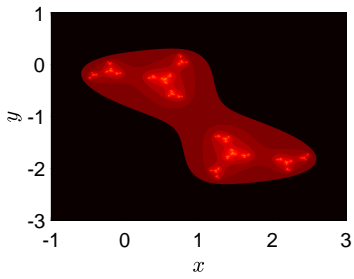
(d) $t = 0.2$

(e) $t = 0.3$
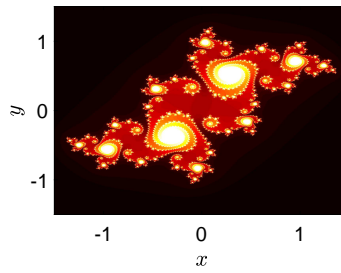

(f) $t = 0.4$

(g) $t = 0.5$

Figure 3.5: The fractal trajectory for (311) and its points

63

(a) $A_t \mathcal{J}$
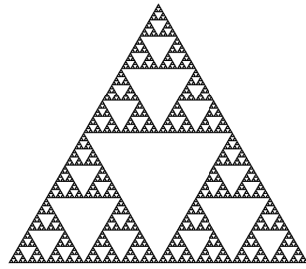

(b) $t = \frac{\pi}{2}$

(c) $t = 2\pi$

Figure 3.6: The parametric set and its sections
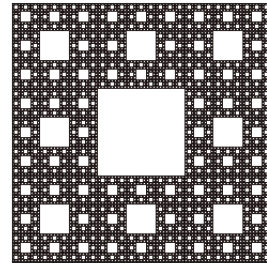
(a) Sierpinski gasket   (b) Sierpinski carpet

Figure 3.7: Sierpinski Fractals

one. Similarly, each next iteration, is a repetition of the same procedure to each of the remaining squares from the preceding iteration. Figure 3.7 shows the two Sierpinski fractals for finite iterations, which are constructed by the methods introduced and discussed in this section.

3.5.1 Construction of the Fractals

The Sierpinski fractals are typically generated using IFS [105, 106], which is defined as a collection of affine transformations. Another way of construction can accomplished by adopting the idea of FJI and developing some schemes for constructing Sierpinski fractals. The technique of the FJI is based on detecting the points of a fractal set through the boundedness of their iterations under a specific map. Here, we shall extend the technique to include any possible criterion for grouping points in a given domain. It is worthy to mention that FJI can be constructed from IFS [24, 106].

3.5.1.1 Sierpinski carpets

At first glance, the Sierpinski carpet seems to be a two dimensional version of the middle third Cantor set. To discuss this thought, let us consider the tent map T defined

65

on the interval $\mathcal{I} = [0, 1]$ such that

$$T(x) = \begin{cases} 3x, & \text{if } x \leq \frac{1}{2}, \\ 3(1-x), & \text{if } x > \frac{1}{2}. \end{cases} \tag{315}$$

The Julia set corresponding to the map (315) is the middle third Cantor set [22]. For planar fractals we consider the FJI defined by the two-dimensional tent map

$$(x_{n+1}, y_{n+1}) = \left(\frac{3}{2} - 3\left|x_n - \frac{1}{2}\right|, \frac{3}{2} - 3\left|y_n - \frac{1}{2}\right| \right), \tag{316}$$

with the initial square $\mathcal{D} = [0, 1] \times [0, 1]$. If we exclude each point (x_0, y_0) whose iterated values (x_n, y_n) escape from $\mathcal{D}$, i.e., at least one coordinate escapes, $x_n > 1$ or $y_n > 1$ for some $n \in \mathbb{N}$, we shall get a Cantor dust. This set is simply the Cartesian product of the Cantor set with itself, and it is a fractal possessing both self-similarity and fractional dimension. Figure 3.8 (a) shows the 3rd approximation of the Cantor dust generated by (316).

Let us now modify this procedure such that a point (x_0, y_0) is excluded from $\mathcal{D}$ if both of its coordinates' iterations (x_n, y_n) escape from the initial set, that is, if $x_n > 1$ and $y_n > 1$ for some $n \in \mathbb{N}$. This procedure for iteration (316) will give a kind of two dimensional Cantor set shown in Fig. 3.8 (b) with the 3rd approximation. More similar object to the Sierpinski carpet can be obtained by considering simultaneous escape of both coordinates, viz., (x_0, y_0) is excluded only if $x_n > 1$ and $y_n > 1$ at the same iteration n. Figure 3.8 (c) shows the 5th approximations of the resulting set. This set is clearly not a fractal from the dimension point of view. The self-similarity is also not satisfied over the whole set. However, a special type of self-similarity can be observed where the corners replicate the whole shape.

The construction of the Sierpinski carpet cannot possibly be performed through any arrangement of two dimensional Cantor set and, therefore, a different strategy should be considered. To this end, we shall use maps that construct sets which are similar to Cantor sets in the generation way but different in structure. A suitable set for generating the Sierpinski carpet started with the initial set $\mathcal{I} = [0, 1]$. The first iteration involves subdividing $\mathcal{I}$ into three equal intervals and removing the middle open interval $(\frac{1}{3}, \frac{2}{3})$. In the second iteration the middle interval is restored and each of the three intervals are again subdivided into three equal subintervals then we remove the

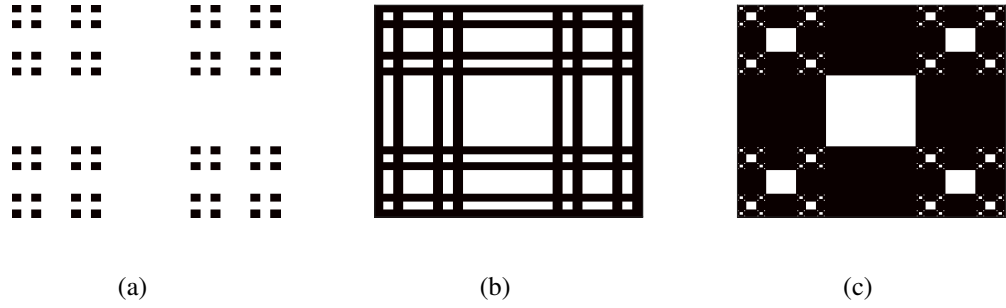(a)   (b)   (c)

Figure 3.8: Approximations of planar sets generated by (316) with different conditions of grouping the points
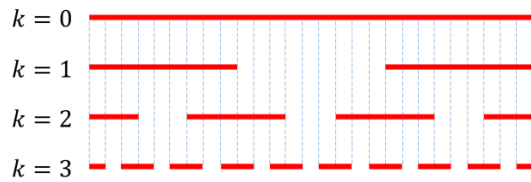
Figure 3.9: Perforation set

middle open intervals $(\frac{1}{9}, \frac{2}{9})$, $(\frac{4}{9}, \frac{5}{9})$, and $(\frac{7}{9}, \frac{8}{9})$. We continue in the same manner for the succeeding iterations. Figure 3.9 illustrates the first three stages of construction of the set. The purpose of such sets is to cut out successively smaller parts (holes) in the Sierpinski fractals kind. This is why we call these types of sets "*perforation sets*".

To construct perforation sets, we use the modified tent map

$$F(x) = \begin{cases} 3\left[x(\text{mod } 1)\right], & \text{if } x \leq \frac{1}{2} \text{ or } x > 1, \\ 3(1-x), & \text{if } \frac{1}{2} < x \leq 1. \end{cases}$$

The point $x \in \mathcal{I}$ is excluded from the kth approximation of the set if its kth iteration $F^k(x)$ does not belong to $\mathcal{I}$. For the Sierpinski carpet we use a two dimensional version of the modified tent map defined on the domain $\mathcal{D} = [0, 1] \times [0, 1]$. We

67

consider the iteration

$$
\begin{aligned}
x_{n+1} &= \begin{cases} 3\left[x_n(\bmod 1)\right], & \text{if } x_n \leq \tfrac{1}{2} \text{ or } x_n > 1, \\[2mm] 3(1 - x_n), & \text{if } \tfrac{1}{2} < x_n \leq 1, \end{cases} \\[3mm]
y_{n+1} &= \begin{cases} 3\left[y_n(\bmod 1)\right], & \text{if } y_n \leq \tfrac{1}{2} \text{ or } y_n > 1, \\[2mm] 3(1 - y_n), & \text{if } \tfrac{1}{2} < y_n \leq 1. \end{cases}
\end{aligned}
\tag{317}
$$

To generate the Sierpinski carpet we exclude any point $(x_0, y_0) \in \mathcal{D}$ if its iteration (x_n, y_n) under (317) escapes from $\mathcal{D}$ such that $x_n > 1$, $y_n > 1$ for some natural number n. Figure 3.7 (b) shows the 6th approximation of the Sierpinski carpet generated by iteration (317). The iteration looks very similar to the FJI but with different criterion for grouping the points. However, it can be classified under FJI type.

Another scheme can be developed by using a map to generate a sequence for each point in a given domain and then applying a suitable criterion to group the points. For that purpose, let us introduce the map

$$
\psi_n(x) = B\sin(A_n x), \tag{318}
$$

where $A_n = \pi a^{n-1}$, $B = \csc \frac{\pi}{b}$, and a, b are parameters. The recursive formula is defined as follows:

$$
\begin{aligned}
\psi_0(x_0) &:= x_0, \\
x_n &= \psi_n(x_0), \ n = 1, 2, \dots .
\end{aligned}
$$

To construct the perforation set, we start with the interval $\mathcal{I} = [0, 1]$, and include in the kth approximation of the set each point $x_0 \in \mathcal{I}$ that satisfies $|x_k| \leq 1$. Thus, for Sierpinski carpet, we use a two dimensional version of the map (318) which can be defined in the form

$$
\psi_n(x, y) = \big(B\sin(A_n x), \ B\sin(A_n y)\big). \tag{319}
$$

The procedure here is to determine the image sequence (x_n, y_n) of each point $(x_0, y_0) \in \mathcal{D}$, i.e.,

$$
(x_n, y_n) = \psi_n(x_0, y_0). \tag{320}
$$

(a) $a = b = 4$ (c) $a = 3$, $b = 4$ (e) $a = 2$, $b = 3.5$

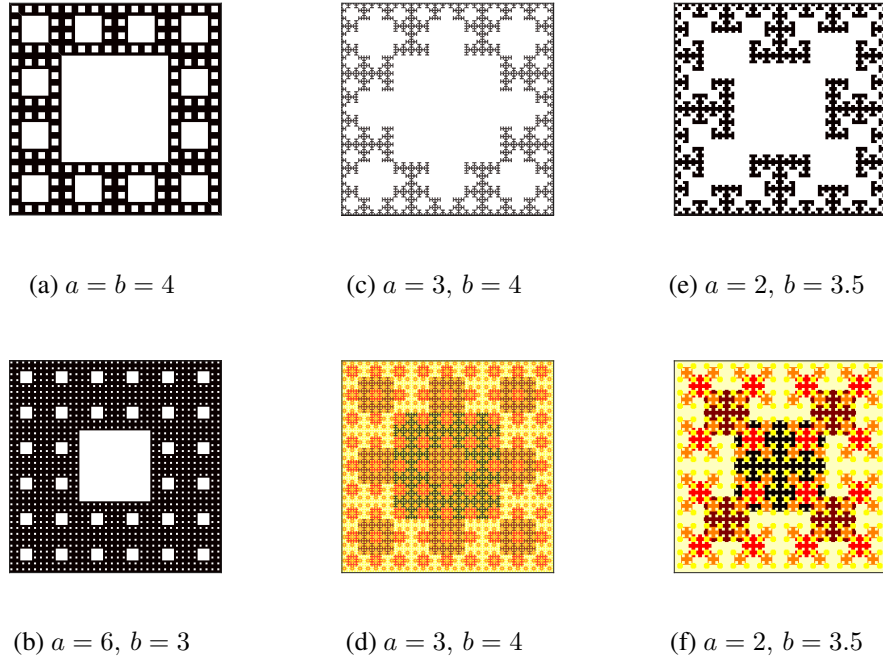(b) $a = 6$, $b = 3$ (d) $a = 3$, $b = 4$ (f) $a = 2$, $b = 3.5$
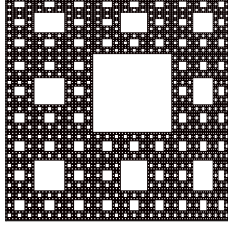
Figure 3.10: Sierpinski Carpets

If we choose $\mathcal{D} = [0, 1] \times [0, 1]$, the point (x_0, y_0) is excluded from the set if the condition

$$|x_n| > 1, \ |y_n| > 1 \qquad (321)$$

is satisfied for some $n \in \mathbb{N}$.

For the values of the parameters $a = 3$ and $b = 3$, the scheme gives the classical Sierpinski carpet (the simulation result for the 6th approximation is identical to Fig. 3.7 (b)). Figure 3.10 shows other carpets generated by (319) with different values of the parameters a and b, and for limited stages. The colors that appear in the parts (d) and (f) of the figure are related to the sequences generated by (320) such that the color of each point in the carpets depends on the smallest number of stages n that satisfies condition (321).

This scheme is quite different than the usual procedure of FJI since iterations are not utilized and a different criterion is applied for grouping the points. However, we shall see later that the idea of the FMI can be applied for this type which allows to map and introduce dynamics for the constructed carpets.
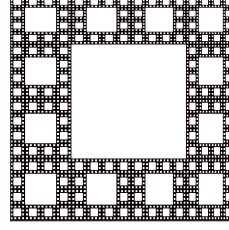
(a) $a = 3$, $b = 3$ (b) $a = 4$, $b = 4$

Figure 3.11: Sierpinski carpets by the FJI (322)

A more similar iteration to that of Fatou and Julia can be constructed by finding the inverse $x = \psi_n^{-1}(x_n)$ in (318) and then substituting in $x_{n+1} = \psi_{n+1}(x)$ to get the autonomous iteration

$$x_{n+1} = B \sin\left(a \sin^{-1} \frac{x_n}{B}\right). \tag{322}$$

The carpets shown in Fig. 3.11 are simulated by using a two dimensional form of iteration (322), and they are irregular types of fractals. These fractals have asymmetric similarities and they are not categorized under random fractals [114].

3.5.1.2 Sierpinski gasket

For constructing the Sierpinski gasket we again use the perforation sets, and in this case we introduce a special coordinate system shown in Fig. 3.12 (a). The system consists of three non-rectangular plane axes denoted by x', x'', and y, and the thick red lines in the figure represent the perforation set constructed in Fig. 3.12 (b).

We start with the initial set $\mathcal{D}$ which is a unit equilateral triangle defined by $\mathcal{D} = \{(x, y) \in \mathbb{R}^2 : \frac{-1}{\sqrt{3}} y \leq x \leq \frac{1}{\sqrt{3}} y, \ 0 \leq y \leq \frac{\sqrt{3}}{2}\}$. For each point $(x, y) \in \mathcal{D}$, we detect the triple (x', x'', y), where x' and x'' are the projections of (x, y) on the x' and x'' axes, respectively. To examine whether the point (x, y) belongs to the gasket, we set up the recursive formula

$$(x_n', x_n'', y_n) = \left(\alpha\big(A_n x'\big), \ \beta\big(A_n x''\big), \ \gamma\big(A_n y\big)\right), \tag{323}$$

where α, β and γ are functions, $A_n = \frac{2}{\sqrt{3}} \pi a^n$, and a is a parameter. The point (x, y)

70
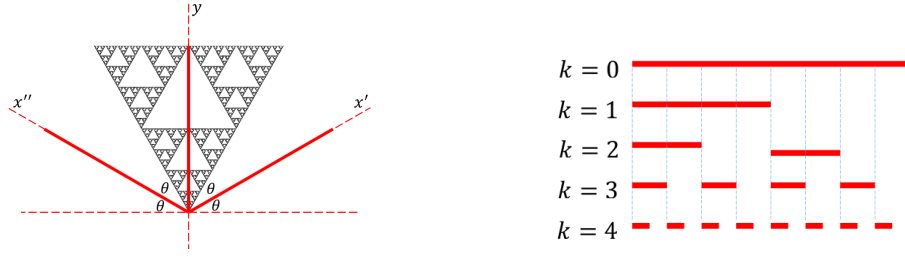
(a) Coordinate system for Sierpinski gasket construction

(b) Perforation set

Figure 3.12: Sierpinski gasket construction

is excluded from the resulting gasket if $x'_n > 0$, $x''_n > 0$ and $y_n < 0$ for some $n \in \mathbb{N}$.

For $\alpha(x) = \beta(x) = \gamma(x) = \sin x$ and $a = 2$, the resulting gasket is the classical Sierpinski gasket. Figure 3.7 (a) shows the 8th approximation of the Sierpinski gasket generated by iteration (323). Examples of other gaskets with different choices of the functions α, β, γ and the parameter a are shown in Fig. 3.13.

3.5.2 Mappings

In this part of the research we give procedures for mapping the Sierpinski fractals through the schemes introduced in the preceding section.

3.5.2.1 Mapping of carpets

To map the carpets generated by the scheme (319), we use the idea of FMI. Let $\Phi : \mathcal{D} \to \mathcal{D}'$ be an invertible function defined by

$$\Phi(x, y) = (\phi_1, \phi_2)(x, y), \tag{324}$$

with the inverse

$$\Phi^{-1}(\xi, \eta) = (\phi_3, \phi_4)(\xi, \eta). \tag{325}$$

Then the fractal mapping scheme can be defined as

$$\Phi^{-1}(\xi_n, \eta_n) = \psi_n\big(\Phi^{-1}(\xi_0, \eta_0)\big). \tag{326}$$

71
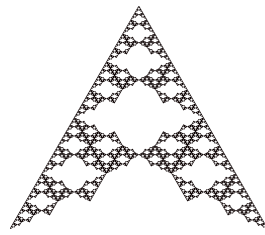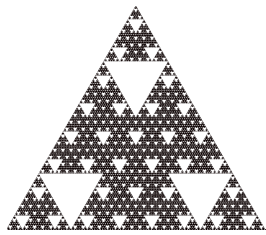
(a) $\alpha(x) = \beta(x) = \gamma(x) = \sin(x)$, $a = 4$
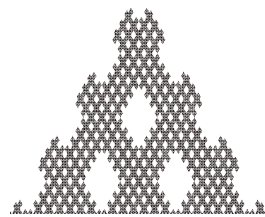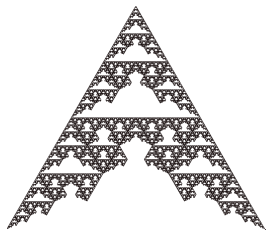
(b) $\alpha(x) = \beta(x) = \gamma(x) = \cos(x)$, $a = 2$

(c) $\alpha(x) = \tan(x)$, $\beta(x) = \gamma(x) = \cos(x)$, $a = 2$

(d) $\alpha(x) = \tan^{-1}(x)$, $\beta(x) = \gamma(x) = \cos(x)$, $a = 7$

Figure 3.13: Sierpinski Gaskets

This scheme transforms a carpet $\mathcal{F}$ into a new carpet $\mathcal{F}_\Phi$, and the following theorem shows that the set $\mathcal{F}_\Phi$ is merely the image of $\mathcal{F}$ under the map Φ.

Theorem 3. $\mathcal{F}_\Phi = \Phi(\mathcal{F})$.

Proof. First, we show that $\mathcal{F}_\Phi \subseteq \Phi(\mathcal{F})$. Let $(\xi, \eta) \in \mathcal{F}_\Phi$, which means that for formula (326), if $(\xi_0, \eta_0) = (\xi, \eta)$, then at least one of $|u_n|$ and $|v_n|$ is less than or equal to 1 for all $n \in \mathbb{N}$, where $(u_n, v_n) = \Phi^{-1}(\xi_n, \eta_n)$. This implies that $(u, v) = (u_0, v_0) \in \mathcal{F}$. Thus $(\xi, \eta) \in \Phi(\mathcal{F})$.

For the reverse inclusion, suppose that $(\xi, \eta) \in \Phi(\mathcal{F})$, i.e., there exists $(x, y) \in \mathcal{F}$ such that $\Phi(x, y) = (\xi, \eta)$ and $(x_0, y_0) = (x, y)$ with formula (320) in which at least one of $|x_n|$ and $|y_n|$ is less than or equal to 1 for all $n \in \mathbb{N}$. This directly implies that the sequence $\Phi^{-1}(\xi_n, \eta_n) = (x_n, y_n)$ satisfies (326) and $(\xi, \eta) \in \mathcal{F}_\Phi$. $\qquad\square$

The following question arises here: Is the mapped carpet a fractal? The answer is "*yes*" if the map Φ satisfies a bi-Lipschitz condition. This result is stated in Lemma 1.

For our next examples, we shall use bi-Lipschitz functions to ensure that the mapped carpets are fractals. In order to obtain the mapped Sierpinski carpet $\mathcal{F}_\Phi$, we restrict the domain of (326) only to the points (ξ, η) that belong to the mapped domain $\mathcal{D}'$, thus Eq. (326) becomes

$$(\xi_n, \eta_n) = \Phi\big(\psi_n(x_0, y_0)\big), \quad (x_0, y_0) \in \mathcal{D}.$$

More precisely, by using Eqs. (319) and (325) in (326), we have

$$\Phi^{-1}(\xi_n, \eta_n) = \left(\frac{\sin(a^{n-1}\pi\phi_3(\xi_0, \eta_0))}{\sin(\frac{\pi}{b})}, \; \frac{\sin(a^{n-1}\pi\phi_4(\xi_0, \eta_0))}{\sin(\frac{\pi}{b})} \right).$$

Now letting $\frac{\sin(a^{n-1}\pi\phi_3(\xi_0, \eta_0))}{\sin(\frac{\pi}{b})} = X_n$ and $\frac{\sin(a^{n-1}\pi\phi_4(\xi_0, \eta_0))}{\sin(\frac{\pi}{b})} = Y_n$ and using Eq. (324), we get

$$(\xi_n, \eta_n) = \Big(\phi_1(X_n, Y_n), \; \phi_2(X_n, Y_n) \Big). \tag{327}$$

The semi-iteration (327) is applied for each point $(\xi_0, \eta_0) \in \mathcal{D}'$, and the point is excluded from the image set $\mathcal{F}_\Phi$ if $|\phi_3(\xi_n, \eta_n)| > 1$, $|\phi_4(\xi_n, \eta_n)| > 1$ for some $n \in \mathbb{N}$. Figures 3.14 and 3.15 show different examples for mappings of carpets by $\Phi(x, y) = (x^2 + y^2, \; x - y)$ and $\Phi(x, y) = (\sin x + y, \; \cos x)$ respectively. The colors displayed in these figures are produced in a similar way to those in Fig. 3.10.
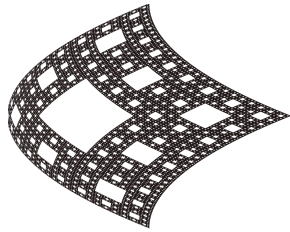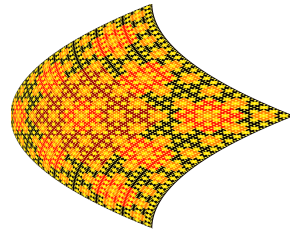
(a)   (b)

Figure 3.14: The images of carpets with (a): $a = b = 3$, (b): $a = 3$, $b = 4$
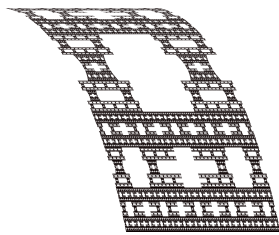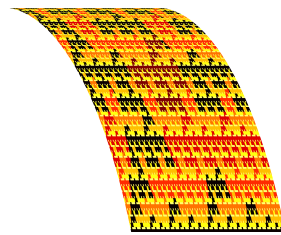
(a)   (b)

Figure 3.15: The image of carpet with (a): $a = 2$, $b = 3.5$, (b): $a = 2$, $b = 1.5$

<div align="center">(a) Image of Sierpinski gasket</div>

(b) Image of gasket with $\alpha(x) = \beta(x) = \gamma(x) = \cos x, \ a = 2$
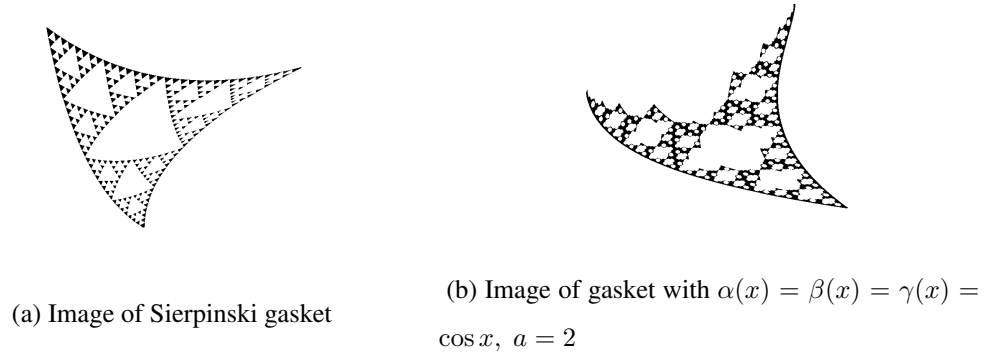
<div align="center">Figure 3.16: Mappings of gaskets</div>

3.5.2.2 Mapping of gaskets

Let us give examples of mappings of gaskets using formula (323). Figure 3.16 (a) shows the mapped Sierpinski gasket by the map $\Phi(x, y) = (x^2 - y, x + y^2)$, whereas Fig. 3.16 (b) represents the mapped gasket depicted in Fig. 3.13 (b) by the map $\Phi(x, y) = (x + y^2, x - 2y^{\frac{2}{3}})$.

3.5.3 Dynamics

Based on the fractal mapping iteration, we introduce dynamics in fractals. As in Subsection 3.4.1, discrete dynamics can be constructed for Sierpinski fractals by iterating the mappings introduced in the previous section. In other words, if we start, for example, with the Sierpinski carpet as an initial set, $\mathcal{S}_0$, and iterate the map Φ in FMI, we shall have the image sets

$$\mathcal{S}_m = \Phi^m(\mathcal{S}_0), \ m = 1, 2, 3, \dots .$$

Thus the discrete dynamics will consist of these fractal sets, $\mathcal{S}_m$, as points of a trajectory.

For continuous dynamics, the idea is to use the motion of a dynamical system with a fractal as an initial set. The motion of dynamical system is defined by $\mathcal{A}_t \mathbf{x}_0 = \varphi(t, \mathbf{x}_0)$, where φ is the solution of a two dimensional system of ordinary differential

<div align="center">75</div>

equations

$$\mathbf{x}' = g(t, \mathbf{x}), \tag{328}$$

with $\varphi(0, \mathbf{x}_0) = \mathbf{x}_0$.

In the case of the Sierpinski carpet, we iteratively apply a motion $\mathcal{A}_t$ to the scheme (319) in the way

$$\mathcal{A}_{-t}(\xi_n, \eta_n) = \psi_n\big(\mathcal{A}_{-t}(\xi, \eta)\big),$$

where $\mathcal{A}_t(x, y) = (A_t x, B_t y)$. Through this procedure, we construct dynamics of sets $A_t \mathcal{F}$, where the Sierpinski carpet $\mathcal{F}$ is the initial value. Thus, the differential equations are involved in fractals such that the latter become points of the solution trajectory. If the map A_t is bi-Lipschitzian (this is true, for instance, if the function g in (328) is Lipschitzian) then the set $A_t \mathcal{F}$ for each fixed t is a fractal.

Let us now consider the Van Der Pol equation

$$u'' + \mu(u^2 - 1)u' + u = 0, \tag{329}$$

where μ is a real constant known as the damping parameter. Using the variables $x = u$ and $y = u'$, one can show that Eq. (329) is equivalent to the autonomous system

$$\begin{aligned} x' &= y, \\ y' &= \mu(1 - x^2)y - x. \end{aligned} \tag{330}$$

Let us denote by $\big(x(t, x_0), y(t, y_0)\big)$ the solution of (330) with $x(0, x_0) = x_0$, $y(0, y_0) = y_0$. System (330) can be numerically solved to construct a dynamical system with the motion $\mathcal{A}_t(x_0, y_0) = (A_t x_0, B_t y_0)$ where $A_t x_0 = x(t, x_0)$ and $B_t y_0 = y(t, y_0)$. We apply this dynamics for an approximation of the Sierpinski Carpet as an initial set. The trajectory of the Van Der Pol dynamics with $\mu = 0.5$ and $0 \le t \le 8$ is shown in Fig. 3.17. Figure 3.18 exhibits the sections of the trajectory at the moments $t = 1, t = 3, t = 5$, and $t = 7$.

In Fig. 3.19 we again show two sections of the trajectory of the Van Der Pol dynamics for the approximation of the Sierpinski Carpet but with $\mu = 1.3$. Comparing these sections with their time counterpart in Fig. 3.18, we can observe the dissimilarity in the deformation rate in the structure of the Sierpinski carpet. This is attributed to that
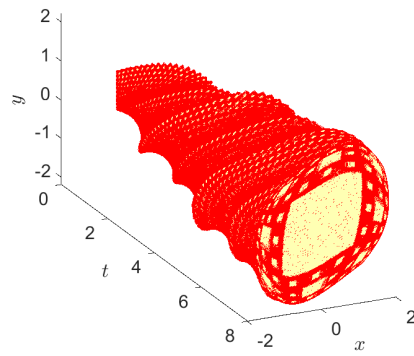
Figure 3.17: Van Der Pol dynamics of Sierpinski carpet
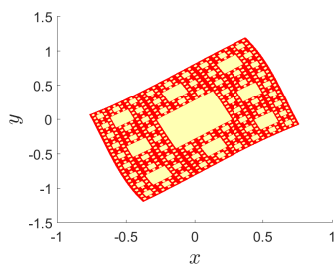
(a) $t = 1$
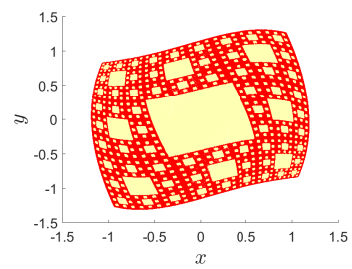
(b) $t = 3$
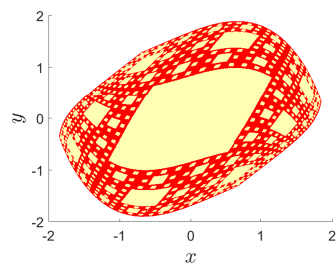
(c) $t = 5$
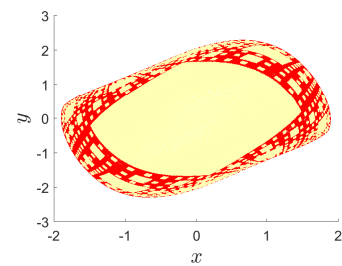
(d) $t = 7$

Figure 3.18: Trajectory sections of the Van Der Pol dynamics in Sierpinski carpet

(a) $t = 1$ (b) $t = 3$
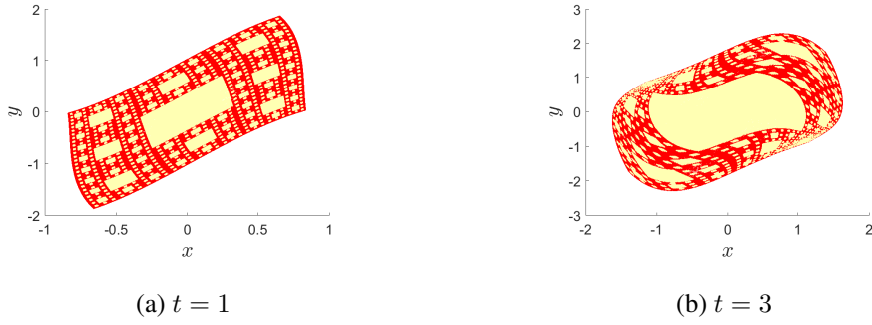
Figure 3.19: Trajectory sections of the Van Der Pol dynamics with $\mu = 1.3$

the value of the damping parameter reflects the degree of nonlinearity of the Van Der Pol equation.

For dynamics in Sierpinski gasket, let us consider the Duffing equation

$$u'' + \delta u' + \beta u + \alpha u^3 = \gamma \cos \omega t,$$

where $\delta, \beta, \alpha, \gamma$, and ω are real parameters. The equation is equivalent to the non-autonomous system

$$x' = y,$$
$$y' = -\delta y - \beta x - \alpha x^3 + \gamma \cos \omega t.$$

In a similar way to the mapping of gasket, we apply the dynamical system associated with the Duffing equation to an approximation of the Sierpinski gasket. The fractal trajectory for $0 \leq t \leq 3$ is shown in Fig. 3.20, whereas Fig. 3.21 displays the sections of the trajectory at the specific times $t = 0.8$, $t = 1.4$, $t = 2.0$, and $t = 2.6$. The values $\delta = 0.08$, $\beta = 0$, $\alpha = 1$, $\gamma = 0.2$ and $\omega = 1$ are used in the simulation.

3.6 Discussions

Despite the intensive research of fractals lasts more than 35 years [2], there are still no results on mapping of the sets, and our research is the first one to consider the problem. To say about mathematical challenges connected to our suggestions, let us start with topological equivalence of fractals and consequently, normal forms. Differential

78
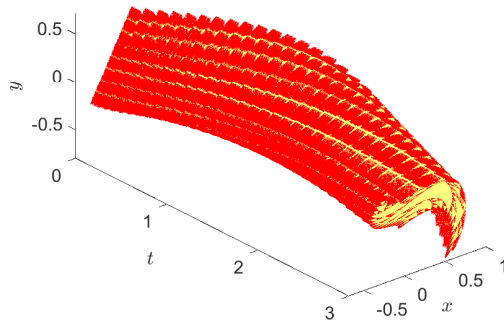
Figure 3.20: Trajectory of the Duffing dynamics in Sierpinski gasket

(a) $t = 0.8$

(b) $t = 1.4$

(c) $t = 2.0$

(d) $t = 2.6$
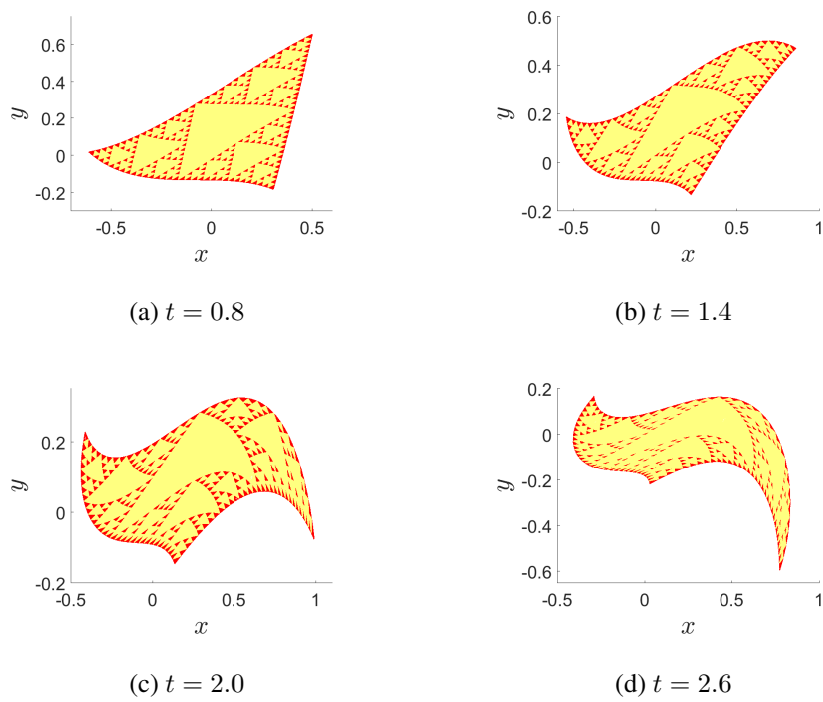
Figure 3.21: Sections of the trajectory

and discrete equations will be analyzed with new methods of fractal dynamics joined with dimension analysis. Next, the theory for dynamical systems which is defined as iterated maps can be developed. Therefore, mapping of fractals will be beneficial for new researches in hyperbolic dynamics, strange attractors, and ergodic theory [115, 116]. The developed approach will enrich the methods for the discovery and construction of fractals in the real world and industry such as nano-fiber engineering, 3D printing, biology, cosmology, biotechnologies, genetics, signal processing, civil engineering, etc. [43, 117, 118, 119, 120, 121].

Let us outline how our results can be useful for applications combined with already existing ones in the area. We start with the theory of scale relativity developed in [122, 123]. In this theory, fractals are considered as a geometric framework of atomic scale motions such that the quantum behavior can be viewed as particles moving on fractal trajectories. One can suppose that by composing the scale relativity theory with dynamics of fractals developed in our research, we will be able to understand better the fractal nature of the world. The expression of a scale-dependent physical quantity requires besides space-time variables, a scale variable. Thus, it is regarded as a fractal function but differentiable when the scale variable is nonzero, therefore, it can be a solution of differential equations involving its derivatives with respect to space-time and scale variables. For a fixed value of the scale variable the solution is a fractal. By varying the scale variable, one can set up an ordinary differential equation to construct a dynamical system. Then, by applying a mapping iteration whose initial set is a scale-dependent physical quantity with fixed a scale variable, one may show that the resulting surface is also a fractal. From another side, fractal dynamics determined by mapping iterations possibly can be a good instrument to study quantum mechanical properties. An example of such properties is the quantum interference of atoms and molecules. Fractal geometry has been used to study the interference patterns of waves such as in electromyography, diffraction grating, and color texture analysis [124, 125, 126]. In our case it would be interesting if one could perform simulations analogous to Young's experiment such that the interference occurs between two fractal trajectories. A possible connection between fractals mappings and quantum mechanics through the scale relativity theory can provide important applications for the former in various fields such as biology, cosmology, and fractal geodesics (see

[123] and the relevant references listed therein).

Further applications can be done with another class of fractal functions which is defined as a family of real functions whose graphs are attractors for IFS [24, 106, 127, 128]. This type is called fractal interpolation function where it is a continuous fractal function interpolating a given set of points [129]. The IFS is defined by a finite collection of affine mappings. The similarity between the IFS and Fatou-Julia iteration (FJI) derives from the fact that both of them consist of infinite long iterations. Moreover, the graphs of some fractal functions constructed by IFS, likewise the Cantor set [128], can also be generated by FJI [22]. Additionally, the graphs of such functions can be mapped to graphs of new fractal functions by fractal mapping iterations and introduce dynamics on these sets. Furthermore, we suppose that the idea of mapping on the basis of FJI can be extended to IFS as they are iterative. Consequently, the results of the present research can be applied to various applications associated with fractal interpolation functions such as signal processing and modeling coastlines and shapes [130, 131, 132, 133, 134].

Owing to the important roles of Sierpinski fractals in several applications like weighted networks, trapping problems, antenna engineering, city planning, and urban growth [135, 136, 137, 138, 139], we expect that the results will be helpful in further fields of applications. One of the relevant applications involves optimization theory. Fractal geometry is used to solve some classes of optimization problems such as supply chain management and hierarchical design [140, 141]. In paper [140], for instance, the properties of a particular hierarchical structure is established. The authors constructed the relationship between the Hausdorff dimension of the optimal structure and loading for which the structure is optimized. The Hausdorff dimension is calculated through considering the self-similarity of the structure at different hierarchical levels. The self-similar fractals, like the Sierpinski gasket, are considered as effective tools for studying the hierarchical structures [137, 142]. Thus, finding a way to map this type of structures allows to create a new hierarchical structure with the same Hausdorff dimension but different mechanical properties if one consider bi-Lipschitz maps.

Finally, but not less important, another application field is partial differential equa-

tions with fractal boundaries [143, 144, 145, 146]. These equations are significantly useful for many fields such as electromagnetics, elasticity theory, and signal processing. For instance, the paper [143] deals with a relevant Brownian motion problem. The boundaries of the problem considered in the paper are of self-similar type such as Koch's snowflake curve. For partial differential equations, one can either apply a fractal mapping iteration extended to continuous dynamics in our research or develop the approach on the basis of IFS. Thus, in the future, one can not only develop numerical solutions of such problems but also confirm that the integral surfaces of the boundary value problems are fractals.

REFERENCES

[1] T. Y. Li and J. A. Yorke, "Period three implies chaos," *Amer. Math. Monthly*, vol. 82, pp. 985–992, (1975).

[2] B. B. Mandelbrot, *Les Objets Fractals: Forme, Hasard, et Dimension*. Paris: Flammarion, 1975.

[3] S. H. Kellert, *In the wake of chaos: Unpredictable order in dynamical systems*. Chicago: University of Chicago Press, 1994.

[4] S. H. Strogatz, *Nonlinear Dynamics and Chaos: With Applications to Physics, Biology, Chemistry, and Engineering*. Reading, Mass: Addison-Wesley Pub, 1994.

[5] J. Tabak, *Probability and Statistics: The Science of Uncertainty*. New York: Facts on File, Inc., 2004.

[6] I. P. Williams and N. Thomas, eds., *Solar and Extrasolar Planetary Systems*. Berlin Heidelberg: Springer-Verlag, 2001.

[7] B. D. Watts, *Clausewitzian Friction and Future War*. Washington, D.C.: National Defense University Press, 2004.

[8] K. K. Tung, *Topics in mathematical modeling*. Princeton, New Jersey: Princeton University Press, 2007.

[9] G. J. Sussman and J. Wisdom, "Numerical evidence that the motion of pluto is chaotic," *Science*, vol. 241, pp. 433–437, (1988).

[10] G. J. Sussman and J. Wisdom, "Chaotic evolution of the solar system," *Science*, vol. 257, pp. 56–62, (1992).

[11] J. Laskar, "Anumerical experiment on the chaotic behaviour of the solar system," *Nature*, vol. 338, pp. 237–238, (1989).

[12] J. Laskar, *Planetary Systems: The Long View*, ch. Physical implications of the chaotic behavior of the Solar System, pp. 191–198. France: Editions Frontieres, 1998.

[13] E. N. Lorenz, "Deterministic nonperiodic flow," *J. Atmos. Sci.*, vol. 20, pp. 130–141, (1963).

[14] R. L. Devaney, *An Introduction to Chaotic Dynamical Systems*. Menlo Park: Addison-Wesley, 1989.

[15] M. J. Feigenbaum, "Universal behavior in nonlinear systems," *Los Alamos Sci./Summer*, vol. 1, pp. 4–27, (1980).

[16] E. Schöll and H. G. Schuster, eds., *Handbook of Chaos Control*. Weinheim. Germany: Wiley–VCH, 2008.

[17] E. Sander and J. A. Yorke, "Period-doubling cascades galore," *Ergod. Theory Dyn. Syst.*, vol. 31, pp. 1249–1267, (2011).

[18] M. Akhmet and M. O. Fen, "Unpredictable points and chaos," *Commun. Nonlinear Sci. Numer. Simulat.*, vol. 40, pp. 1–5, (2016).

[19] M. Akhmet and M. O. Fen, "Poincaré chaos and unpredictable functions," *Commun. Nonlinear Sci. Numer. Simulat.*, vol. 48, pp. 85–94, (2016).

[20] B. B. Mandelbrot, *The Fractal Geometry of Nature*. New York: Freeman, 1983.

[21] O. Zmeskal, P. Dzik, and M. Vesely, "Entropy of fractal systems," *Comput. Math. Appl.*, vol. 66, pp. 135–146, (2013).

[22] B. B. Mandelbrot, *Fractals and Chaos: The Mandelbrot Set and Beyond*. New York: Springer, 2004.

[23] F. C. Moon, *Chaotic and Fractal Dynamics: An Introduction for Applied Scientists and Engineers*. New York: Wiley, 1992.

[24] M. F. Barnsley, *Fractals Everywhere: New Edition*. New York: Dover Publication Inc., 2012.

[25] M. Chen, D. Zhou, and Y. Shang, "Nonlinear feedback control of Lorenz system," *Chaos Soliton. Fract.*, vol. 21, pp. 295–304, (2004).

[26] C. Ercai, "Chaos for the sierpinski carpet," *Adv. Mat. Res.*, vol. 88(3/4), pp. 979–984, 1997.

[27] M. U. Akhmet and M. O. Fen, "Replication of chaos," *Commun. Nonlinear Sci. Numer. Simulat.*, vol. 18, pp. 2626–2666, (2013).

[28] M. U. Akhmet and M. O. Fen, *Replication of Chaos in Neural Networks, Economics and Physics*. Berlin, Heidelberg: Springer/HEP, 2016.

[29] J. M. Gonzales-Miranda, *Synchronization and control of chaos*. London: Imperial College Press, 2004.

[30] L. M. Pecora and T. L. Carroll, "Synchronization in chaotic systems," *Phys. Rev. Lett.*, vol. 64, p. 821–824, 1990.

[31] D. Eroglu, J. S. W. Lamb, and T. Pereira, "Synchronisation of chaos and its applications," *Contemp. Phys.*, vol. 58(3), pp. 207–243, 2017.

[32] S. Boccaletti, J. Kurths, G. Osipov, D. L. Valladares, and C. S. Zhou, "The synchronization of chaotic systems," *Phys. Rep.*, vol. 366, p. 1–101, 2002.

[33] M. Akhmet and M. O. Fen, "Extension of Lorenz unpredictability," *Int. J. Bifurcat. Chaos*, vol. 25, no. 10, p. 1550126, (2015).

[34] M. Akhmet and M. O. Fen, "Non-autonomous equations with unpredictable solutions," *Commun. Nonlinear Sci. Numer. Simulat.*, vol. 59, pp. 657–670, (2018).

[35] E. W. Mitchell and S. R. Murray, eds., *Classification and Application of Fractals: New Research*. New York: Nova Science Publishers Inc., 2012.

[36] H. O. Peitgen, H. Jürgens, and D. Saupe, *Chaos and Fractals*. New York: Springer-Verlag, 2004.

[37] B. Y. Sternin and V. E. Shatalov, *Differential Equations on Complex Manifolds*. Dordrecht: Kluwer Academic Publishers, 1994.

[38] M. Batty and P. A. Longley, *Fractal Cities: A Geometry of Form and Function*. London: Academic Press, 1994.

[39] J. A. Kaandorp, *Fractal Modelling: Growth and Form in Biology*. New York: Springer, 2012.

[40] L. Zhao, W. Li, L. Geng, and Y. Ma, *Advances in Automation and Robotics 2, Lecture Notes in Electrical Engineering 123*, ch. Artificial Neural Networks Based on Fractal Growth, pp. 323–330. Berlin: Springer, 2011.

[41] M. Takayasu and H. Takayasu, *Complex Systems in Finance and Econometrics*, ch. Fractals and Economics, pp. 444–463. New York: Springer, 2011.

[42] L. Pietronero and E. Tosatti, *Fractals in Physics*. Amsterdam: North-Holland, 2012.

[43] J. L. Vehel, E. Lutton, and C. Tricot, eds., *Fractals in Engineering: From Theory to Industrial Applications*. New York: Springer, 1997.

[44] P. Fatou, "Sur les équations fonctionnelles, I, II, III," *Bull. Soc. Math. France*, vol. 47, 48, pp. 161–271, 33–94, 208–314, 1919, 1920.

[45] J. Kigami, *Analysis on Fractals*. Cambridge: Cambridge Univ. Press, 2001.

[46] R. S. Strichartz, *Differential Equations on Fractals: A Tutorial*. Princeton: Princeton University Press, 2006.

[47] T. Vicsek, *Fractal Growth Phenomena*. Singapore: World Scientific, 1992.

[48] A. L. Barabasi and H. E. Stanley, *Fractal Concepts in Surface Growth*. Cambridge: Cambridge University Press, 1995.

[49] G. Julia, "Mémoire suv i'itération des fonctions rationelles," *J. Math. Pures Appl.*, vol. 8, pp. 47–245, 1918.

[50] G. K. Vallis, "El Niño: A chaotic dynamical system?," *Science*, vol. 232, pp. 243–245, (1986).

[51] G. K. Vallis, "Conceptual models of El Niño and the southern oscillation," *J. Geophys.*, vol. 93, pp. 13979–13991, (1988).

[52] S. Sen Roy and R. B. Singh, *Climate Variability, Extreme Events and Agriculture Productivity in Mountain Regions*. New Delhi: Oxford and 1BH Publication, 2002.

[53] J. F. Petersen, D. Sack, and R. E. Garbler, *Physical Geography*. Boston: Cengage Learning, 2017.

[54] L. Eppelbaum, I. Kutasov, and A. Pilchin, *Applied Geothermics, Lecture Notes in Earth System Sciences*. Berlin: Springer-Verlag, 2014.

[55] J. Schmandt, J. Clarkson, and G. R. North, *The Impact of Global Warming on Texas*. Austin, Texas: University of Texas Press, 1 ed., 2011.

[56] M. Akhmet and M. O. Fen, "Existence of unpredictable solutions and chaos," *Turk. J. Math.*, vol. 41, pp. 254–266, (2017).

[57] R. C. Robinson, *An Introduction to Dynamical Systems: Continuous and Discrete*. USA: American Mathematical Society, 2 ed., 2012.

[58] F. M. Selten, F. J. Schevenhoven, and G. S. Duane, "Simulating climate with a synchronization-based supermodel," *Chaos*, vol. 27 (12), p. 126903, (2017).

[59] M. L. Shen, N. Keenlyside, B. C. Bhatt, and G. S. Duane, "Role of atmosphere-ocean interactions in supermodeling the tropical Pacific climatel," *Chaos*, vol. 27 (12), p. 126704, (2017).

[60] B. P. Kirtman, N. Perlin, and L. Siqueira, "Ocean eddies and climate predictability," *Chaos*, vol. 27 (12), p. 126902, (2017).

[61] G. Siedler, J. Church, and J. Gould, eds., *Ocean Circulation and Climate: Observing and Modelling the Global Ocean*. San Fransisco: Academic Press, 2001.

[62] V. Barale and M. Gade, *Remote Sensing of the European Seas*. B.V.: Springer Science Business Media, 2008.

[63] M. F. Stuecker, F. F. Jin, and A. Timmermann, "El Niño-Southern Oscillation frequency cascade," *Proc. Natl. Acad. Sci. U.S.A*, vol. 112, pp. 13490–13495, (2015).

[64] J. Bjerknes, "Atmospheric teleconnections from the equatorial Pacific," *Mon. Weather Rev.*, vol. 97, pp. 163–172, (1969).

[65] D. P. Chambers, B. D. Tapley, and R. H. Stewart, "Anomalous warming in the Indian ocean coincident with El Niño," *J. Geophys. Res.*, vol. 104, pp. 3035–3047, (1999).

[66] D. Eamus, A. Huete, and Q. Yu, *Vegetation Dynamics: A Synthesis of Plant Ecophysiology, Remote Sensing and Modelling*. New York: Cambridge University Press, 2016.

[67] T. Yamagata, S. K. Behera, J. J. Luo, S. Masson, M. R. Jury, and S. A. Rao, "Coupled ocean–atmosphere variability in the tropical Indian ocean, Earth's climate: The ocean–atmosphere interaction," *Geophys. Monogr.*, vol. 147, pp. 189–212, (2004).

[68] J. J. Luo, R. C. Zhang, S. K. Behera, Y. Masumoto, F. F. Jin, R. Lukas, and T. Yamagata, "Interaction between El Niño and extreme Indian Ocean Dipole," *J. Climate*, vol. 23, pp. 726–742, (2010).

[69] S. K. Behera, J. J. Luo, S. Masson, S. A. Rao, H. Sakuma, and T. Yamagata, "A CGCM study on the interaction between IOD and ENSO," *J. Climate*, vol. 19, pp. 1688–1705, (2006).

[70] M. Roxy, S. Guladi, H. K. L. Drobhlar, and A. Navarra, "Seasonality in the relationship between El Niño and Indian Ocean Dipole," *Clim. Dyn.*, vol. 37, p. 221–236, (2011).

[71] C. Rosenzweig and D. Hillel, *Climate Variability and the Global Harvest: Impact of El Niño and other Oscillations on Agro-Ecosystems*. New York: Oxford University Press, 2008.

[72] M. Vuille and R. D. Garreaud, *The SAGE Handbook of Environmental Change*, ch. Ocean-Atmosphere Interactions on Interannual to Decadal Time Scales, pp. 471–496. London: Sage, 2011.

[73] C. Lehr, P. J. Ward, and M. Kummu, "Impact of large-scale climatic oscillations on snowfall-related climate parameters in the world's major downhill ski areas: A review," *Mt. Res. Dev.*, vol. 32, pp. 431–445, (2012).

[74] L. Bunge and A. J. Clarke, "A verified estimation of the El Niño index Niño-3.4 since 1877," *J. Climate*, vol. 22, pp. 3979–3992, (2009).

[75] N. A. Rayner, D. E. Parker, H. E. B., C. K. Folland, L. V. Alexander, D. P. Rowell, E. C. Kent, and A. Kaplan, "Global analyses of sea surface temperature, sea ice, and night marine air temperature since the late nineteenth century," *J. Geophys. Res*, vol. 108, no. D14, p. 4407, (2003).

[76] J. Sheinbaum, "Current theories on El Niño-Southern Oscillation: A review," *Geofís. Int*, vol. 42, no. 3, pp. 291–306, (2003).

[77] J. D. Neelin and M. Latif, "El Niño dynamics," *Phys. Today*, vol. 51, no. 12, pp. 32–36, (1998).

[78] E. Tziperman, L. Stone, M. A. Cane, and H. Jarosh, "El Niño chaos: Overlapping of resonance between the seasonal cycle and the Pacific ocean-atmosphere oscillator," *Science*, vol. 264, pp. 72–74, (1994).

[79] D. S. Battisti, "Dynamics and thermodynamics of a warming event in a coupled tropical atmosphere–ocean model," *J. Atmos. Sci.*, vol. 45, pp. 2889–2919, (1988).

[80] C. Penland and L. Matrasova, "A balance condition for stochastic numerical models with application to the El Niño-Southern Oscillationl," *J. Climate*, vol. 7, pp. 1352–1372, (1994).

[81] S. E. Zebiak and M. A. Cane, "A model El Niño-Southern Oscillation," *Mon. Wea. Rev.*, vol. 115, pp. 2262–2278, (1987).

[82] M. Münnich, M. A. Cane, and S. E. Zebiak, "A study of self-excited oscillations in a tropical ocean–atmosphere system, Part II: Nonlinear cases," *J. Atmos. Sci.*, vol. 48, pp. 1238–1248, (1991).

[83] J. Willebrand and D. L. T. Anderson, eds., *Modelling Oceanic Climate Interactions*. Berlin Heidelberg: Springer-Verlag, 1993.

[84] L. E. Lucas, D. E. Waliser, and R. Murtugudde, "Mechanisms governing sea surface temperature anomalies in the eastern tropical Pacific ocean associ-

ated with the boreal winter Madden-Julian oscillation," *JGR-Oceans*, vol. 115, p. C05012, (2010).

[85] W. S. Kessler, L. M. Rothstein, and D. Chen, "The annual cycle of SST in the eastern tropical Pacific as diagnosed in an OGCM," *J. Climate*, vol. 11, pp. 777–799, (1998).

[86] P. R. Gent and M. A. Cane, "A reduced gravity, primitive equation model of the upper equatorial ocean," *J. Comput. Phys.*, vol. 81, pp. 444–480, (1989).

[87] J. W. Stevenson and P. P. Niiler, "Upper ocean heat budget during the Hawaii-to-Tahiti Shuttle Experiment," *J. Phys. Oceanogr.*, vol. 13, pp. 1894–1907, (1983).

[88] M. Jochum and R. Murtugudde, "Temperature advection by tropical instability waves," *J. Phys. Oceanogr.*, vol. 36, pp. 592–605, (2006).

[89] B. N. Saji, N. H.and Goswami, P. N. Vinayachandran, and T. Yamagata, "A dipole mode in the tropical Indian ocean," *Nature*, vol. 401, pp. 360–362, (1999).

[90] R. Lukas and E. Lindstrom, "The mixed layer of the western equatorial Pacific ocean," *J. Geophys. Res.*, vol. 96, pp. 3343–3357, (1991).

[91] G. R. Sell, *Topological Dynamics and Ordinary Differential Equations*. London: Nostrand-Reinhold, 1971.

[92] T. Stocker, *Introduction to Climate Modelling*. Berlin: Springer-Verlag, 2011.

[93] E. Ott, C. Grebogi, and J. A. Yorke, "Controlling chaos," *Phys. Rev. Lett.*, vol. 64, pp. 1196–1199, (1990).

[94] K. Pyragas, "Continuous control of chaos by self-controlling feedback," *Phys. Lett. A*, vol. 170, pp. 421–428, (1992).

[95] R. Saravanan, *Large-Scale Disasters: Prediction, Control, and Mitigation*, ch. Seasonal-to-Decadal Prediction Using Climate Models: Successes and Challenges, pp. 318–328. New York: Cambridge University Press, 2008.

[96] D. Coley, *Energy and Climate Change: Creating a Sustainable Future*. Chichester. UK: John Wiley and Sons, 2008.

[97] S. M. Hammel, J. A. Yorke, and C. Grebogi, "Do numerical orbits of chaotic dynamical processes represent true orbits," *J. Complexity*, vol. 3, pp. 136–145, (1987).

[98] F. Bonjean, "Influence of sea currents on the sea surface temperature in the tropical Pacific ocean," *J. Phys. Oceanogr.*, vol. 31, pp. 943–961, (2001).

[99] B. M. Garay and B. Indig, "Chaos in Vallis' asymmetric Lorenz model for El Niño," *Chaos Soliton. Fract.*, vol. 75, pp. 253–262, (2015).

[100] B. S. T. Alkahtani and A. Atangana, "Chaos on the Vallis model for El Niño with fractional operators," *Entropy*, vol. 18, p. 100, (2016).

[101] M. Borghezan and P. C. Rech, "Chaos and periodicity in Vallis model for El Niño," *Chaos Soliton. Fract.*, vol. 97, pp. 15–18, (2017).

[102] B. Gallego and P. Cessi, "Exchange of heat and momentum between the atmosphere and the ocean: a minimal model of decadal oscillations," *Clim. Dyn.*, vol. 16, pp. 479–489, (2000).

[103] C. Sparrow, *The Lorenz Equations: Bifurcations, Chaos and Strange Attractors*. New York: Springer-Verlag, 1982.

[104] H. T. Yau and C. L. Chen, "Chaos control of Lorenz systems using adaptive controller with input saturation," *Chaos Soliton. Fract.*, vol. 34, pp. 1567–1574, (2007).

[105] J. Hutchinson, "Fractals and self-similarity," *Indiana Univ. J. Math.*, vol. 30, pp. 713–747, 1981.

[106] M. F. Barnsley and S. Demko, "Iterated function systems and the global construction of fractals," *Proc. Roy. Soc. London Ser. A.*, vol. 399, pp. 243–275, 1985.

[107] J. Encarnacao, H. O. Peitgen, G. Saka, and G. Englert, *Fractal Geometry and Computer Graphics*. Berlin: Springer, 1992.

[108] H. O. Peitgen and D. Saupe, eds., *The Science of Fractal Images*. New York: Springer-Verlag, 1988.

[109] A. Goswami, *The Physicists' View of Nature, Part 1: From Newton to Einstein*. Berlin: Springer, 2000.

[110] K. J. Smith, *The Nature of Mathematics*. Boston: Cengage Learning, 2017.

[111] L. V. Ahlfors, *Lectures on Quasiconformal Mappings*. Providence, RI: Amer. Math. Soc., 2 ed., 2006.

[112] K. Falconer, *Fractal Geometry: Mathematical Foundations and Applications*. Chichester: Wiley, 2 ed., 2003.

[113] M. Shishikura, "The hausdorff dimension of the boundary of the mandelbrot set and julia sets," *Ann. of Math.*, vol. 147(2), pp. 225–267, 1998.

[114] D. P. Feldman, *Chaos and Fractals: An Elementary Introduction*. UK: Oxford University Press, 2012.

[115] S. Wiggins, ed., *Global Bifurcation and Chaos: analytical methods*. New York: Springer-Verlag, 1988.

[116] J. Guckenheimer, J. Moser, and S. E. Newhouse, eds., *Dynamical Systems*. Boston: Birkhauser, 1980.

[117] X. Y. Liu and P. D. Sawant, "Determination of the fractal characteristic of nanofiber-network formation in supramolecular materials," *Chem. Phys. Chem.*, vol. 4, pp. 374–377, 2002.

[118] C. Cattani, "Fractals and hidden symmetries in DNA," *Math. Prob. Eng.*, vol. 2010, pp. 1–31, 2010.

[119] R. Noorani, ed., *3D Printing: Technology, Applications, and Selection*. New York: CRC Press, 2017.

[120] G. W. Wornell, *Signal Processing with Fractals: A Wavelet-Based Approach*. Upper Saddle River, NJ: Prentice-Hall, 1996.

[121] P. Frankhauser, "Fractals geometry of urban patterns and their morphogenesis," *Discrete Dynamics in Nature and Society*, vol. 2, pp. 127–145, 1998.

[122] L. Nottale, *Fractal Space-Time and Microphysics Towards a Theory of Scale Relativity*. Singapore: World Scientific, 1993.

[123] L. Nottale, *Scale Relativity and Fractal Space-Time: A New Approach in Unifying Relativity and Quantum Mechanics*. London: Imperial College Press, 2011.

[124] Z. Xu and S. Xiao, "Fractal dimension of surface emg and its determinants," in *The 19th Annual International Conference of the IEEE Engineering in Medicine and Biology Society*, vol. 4, pp. 1570–1573, 1997.

[125] D. Bak, S. P. Kim, S. K. Kim, K. S. Soh, and J. H. Yee, "Fractal diffraction grating," *ArXiv Physics e-prints*, 1998.

[126] D. Casanova, J. B. Florindo, F. M., and O. M. Bruno, "Texture analysis using fractal descriptors estimated by the mutual interference of color channels," *Inf Sci.*, vol. 346-347, pp. 58–72, 2016.

[127] P. R. Massopust, *Fractal Functions, Fractal Surfaces, and Wavelets*. San Diego: Academic Press, 1994.

[128] P. R. Massopust, "Fractal functions and their applications," *Chaos Soliton. Fract.*, vol. 8(2), pp. 171–190, 1997.

[129] D. C. Luor, "Fractal interpolation functions with partial self similarity," *J. Math. Anal. Appl.*, vol. 464, pp. 911–923, 2018.

[130] D. S. Mazel, "Representation of discrete sequences with three-dimensional iterated function systems," *IEEE Trans. Signal Process*, vol. 42, pp. 3269–3271, 1994.

[131] M. Y. Zhai, J. L. Fernández-Martinez, and J. W. Rector, "A new fractal interpolation algorithm and its applications to self-affine signal reconstruction," *Fractals*, vol. 19, pp. 355–365, 2011.

[132] P. Manousopoulos, V. Drakopoulos, and T. Theoharis, "Parameter identification of 1d recurrent fractal interpolation functions with applications to imaging and signal processing," *J. Math. Imaging Vision*, vol. 40, pp. 162–170, 2011.

[133] W. O. Cochran, J. C. Hart, and P. J. Flynn, "On approximating rough curves with fractal functions," *Proc. Graphics Interface.*, vol. 1, pp. 65–72, 1998.

[134] P. Manousopoulos, V. Drakopoulos, and T. Theoharis, "Curve fitting by fractal interpolation," in *Transactions on Computational Science I. Lecture Notes in Computer Science* (M. L. Gavrilova and C. Tan, eds.), vol. 4750, pp. 85–103, Berlin, Heidelberg: Springer, 2008.

[135] Y. Dong, M. Dai, and D. Ye, "Non-homogeneous fractal hierarchical weighted networks," *Plos One*, vol. 10(4), p. e0121946, 2015.

[136] Z. Zhang, Y. Li, S. Gao, S. Zhou, J. Guan, and M. Li, "Trapping in scale-free networks with hierarchical organization of modularity," *Phys. Rev. E*, vol. 80, p. 051120, 2009.

[137] J. J. Kozak and V. Balakrishnan, "Analytic expression for the mean time to absorption for a random walker on the sierpinski gasket," *Phys. Rev. E*, vol. 65, p. 021105, 2002.

[138] A. Kansal and J. Kaur, "Sierpinski gasket fractal array antenna," *IJCSC*, vol. 1(2), pp. 133–136, 2010.

[139] D. Triantakonstantis, "Urban growth prediction modelling using fractals and theory of chaos," *Open J. Civil Eng.*, vol. 2(2), pp. 81–86, 2012.

[140] D. Rayneau-Kirkhope, Y. Mao, and R. Farr, "Optimization of fractal space frames under gentle compressive load," *Phys. Rev. E*, vol. 87, p. 063204, 2013.

[141] S. Liu, H. Dong, and W. Zhao, "Optimization model based on the fractal theory in supply chain management," *Adv. Mat. Res.*, vol. 694-697, pp. 3554–3557, 2013.

[142] J. A. Riera, "Relaxation of hierarchical models defined on sierpinski gasket fractals," *J. Phys. A: Math. Gen.*, vol. 19, pp. L869–L873, 1986.

[143] A. Jonsson and H. Wallin, "Boundary value problems and brownian motion on fractals," *Chaos Soliton. Fract.*, vol. 8(2), pp. 191–205, 1997.

[144] A. P. Pancheha, A. A. Puzenko, and S. A. Puzenko, "Boundary conditions for the electromagnetic field on a non-differentiable fractal surface," *Phys. Lett. A*, vol. 182(4-6), pp. 407–410, 1993.

[145] G. Franceschetti, A. Iodice, D. Riccio, and G. Ruello, "Fractal surfaces and electromagnetic extended boundary conditions," *IEEE Transactions on Geoscience and Remote Sensing*, vol. 40(5), pp. 1018–1031, 2002.

[146] F. M. Borodich and A. Y. Volovikov, "Surface integrals for domains with fractal boundaries and some applications to elasticity," *Proc. Royal Soc. Ser. A*, vol. 456, pp. 1–24, 2000.

CURRICULUM VITAE

PERSONAL INFORMATION

Surname, Name: Alejaily, Ejaily

Nationality: Libyan

Date and Place of Birth: 23.06.1974, Libya

Marital Status: Married

E-mail: ejailymilad@yahoo.com

EDUCATION

Degree	Institution	Year of Graduation
M.Sc.	Universiti Teknologi Malaysia	2009
B.Sc.	Sirte University	1997
High School	Houn Secondary School	1992

PROFESSIONAL EXPERIENCE

Year	Place	Enrollment
2014 – present	College of Engineering Technology (Houn)	Lecturer
2012 – 2014	Misurata University	Lecturer
2010 – 2012	College of Engineering Technology (Houn)	Lecturer
2000 – 2006	College of Engineering Technology (Houn)	Teaching Assistant

PUBLICATIONS

1. E. M. A. Alejaily, *A Boundary Integral Equation for the Neumann Problem in Bounded Multiply Connected Region*, Master Thesis, UTM, 2009.

2. M. M. S. Nasser, A. H. M. Murid, M. Ismail and E. M. A. Alejaily, *Boundary integral equation with the generalized Neumann kernel for Laplace's equation in multiply*

connected regions, Appl. Math. Comput. 217:4710–4727, 2011.

3. M. Akhmet, M. O. Fen and E. M. Alejaily, *Mapping Fatou-Julia Iterations*, Proceeding ICIME 2018, 64-67, 2018.

4. M. Akhmet, M. O. Fen and E. M. Alejaily, *Extension of sea surface temperature unpredictability*, Ocean Dynamics, 69:145–156, 2019.

5. M. Akhmet, M. O. Fen and E. M. Alejaily, *Generation of fractals as Duffing equation orbits*, Chaos, 29(5):053113, 2019.